TÉCNICO LISBOA

Study of Deposition Strategies of a Wire + Arc Additive Manufactured Component

Maria Inês Castro e Silva

Thesis to obtain the Master of Science Degree in

Materials Engineering

Supervisors: Prof. Eurico Gonçalves Assunção

Prof.ª Maria Luísa Coutinho Gomes de Almeida

Examination Committee:

Chairperson: Prof. Pedro Miguel Amaral

Supervisor: Prof. Eurico Gonçalves Assunção

Member of the committee: Dr. Filomeno Martina

Member of the committee: Prof.ª Inês da Fonseca Pestana Asceso Pires

May 2018

Acknowledgements

I would like to express my sincere gratitude to Professor Luisa Coutinho and to Professor Eurico Assunção and Dr. Filomeno Martina for the opportunity given.

A special appreciation goes to all members of the Welding Engineering and Laser Processing Centre in Cranfield University, with more emphasis to Mr. Steve Pope, Mr. Flemming Nielsen and Mr. Nisar Shah for all the technical assistance during the experimental work.

To Leonor Neto, Eloïse Eimer, Júlio Coroado, Gonçalo Pardal, Armando Caballero and Daniela Martegiani, who always had a friendly word, inspired and motivated me to push myself and enjoy scientific investigation. You made me feel like home. To all of you I only wish the best.

To my volleyball foster family: Tomek, Kostas, Ana, Ari and specially, to Cristina and Janis. An enormous thank you.

To my friends who have been supportive and with whom I spent this wonderful experience, with its mostly-ups and downs, Miguel Carreiro, André Farinha, Melissa Costa, Helena Ferreira, André Ruza, a special thank you to all. You've made my journey one that I don't want to forget.

Most importantly, I would like to dedicate this thesis to my grandparents, who've always been supportive of me and my choices, and to my amazing mother, my role model, for encouragement and support on every occasion of my life, making me the person I am today.

Abstract

Fabrication of metal parts by wire and Arc Additive Manufacturing (WAAM) has received an increased interest in recent years, as it allows high design flexibility and reduction of material wastage compared to other traditional manufacturing routes. In this study, a bulk complex structure was made by WAAM, using different deposition strategies, in aluminium 2319, to understand the influence of deposition strategies in porosity, microstructure, microhardness, path efficiency and substrate deformation. Samples were built by using different oscillation deposition paths, with alternating current plasma arc welding power source (ACPAW). This technology is a relatively new and promising for welding aluminium due to its efficient oxide cleaning capability and reduction of porosity when compared to the Cold Metal Transfer (CMT) process. A WAAM software, being developed by Cranfield University, was employed efficiently to program the chosen tool paths. The deposited parts displayed similar microhardness results which were consistent with the achieved microstructure. The average pore diameter size for the deposition strategies was in the range of 16.2 µm to 25.7 µm. The most suitable deposition strategy for the part in study was proposed. Additionally, the substrate deformation results showed that the deposition strategies will have an influence on the residual stresses distribution. It has been shown that using an ACPAW power source for deposition of WAAM meter scale parts of aluminium alloys can be achieved.

Keywords: AA2319, alternating current plasma arc welding, aluminium alloy, complex geometry, deposition paths, microhardness, microstructure, optimization methods, oscillation strategy, part efficiency, porosity, WAAM software, wire and arc additive manufacturing.

Resumo

O fabrico de peças metálicas através da técnica de manufatura aditiva, *Wire and Arc Additive Manufacturing (WAAM),* tem recebido um interesse exponencial recentemente, por permitir uma alta flexibilidade de design de peças e reduzir o desperdício de matéria-prima, quando comparado com outras técnicas de manufatura tradicional. Neste estudo, variadas deposições de uma estrutura compacta e complexa foram realizadas, utilizando como matéria-prima a liga de alumínio 2319, com o auxílio de uma fonte de potência de soldadura em plasma, com polaridade de corrente alternada (ACPAW). Foi também investigado o efeito de estratégias de deposição no aparecimento de porosidade, na microdureza, na eficiência de caminho de deposição e deformação de substrato. A tecnologia implementada é relativamente recente e promissora na deposição de alumínio devido à remoção de óxidos de forma eficiente e pela redução de porosidade quando comparado com a variante de soldadura MIG, o processo de *Cold Metal Transfer* (CMT). Um software desenvolvido pela Universidade de Cranfield foi utilizado para a programação do caminho de deposição. As partes depositadas exibiram valores de microdureza semelhantes entre si, o que foi consistente com os resultados microestruturais. Os diâmetros médios das porosidades encontram-se na gama de valores 16.2 μm a 25.7 μm. A estratégia de deposição mais promissora foi proposta. Adicionalmente, os resultados de deformação do substrato mostraram que as estratégias de deposição vão ter uma alta influência na distribuição de tensões residuais. Foi demonstrado que a utilização de ACPAW para componentes de grandes dimensões é exequível.

Palavras-Chave: AA2319, eficiência, estratégias de deposição, estratégia de oscilação, geometria complexa, liga de alumínio, métodos de optimização, microdureza, microestrutura, porosidade, software de WAAM, soldadura por plasma em corrente alterna, wire and arc additive manufacturing

Contents

List of Figures

List of Tables

Acronyms

AM	Additive Manufacturing
ACPAW	Alternate Current Plasma Arc Welding
AC	Alternating Current
CMT	Cold Metal Transfer
CMT-PADV	Cold Metal Transfer - Pulse Advanced
CAD	Computer-Aided Design
CTWD	Contact Tip to Work Distance
DCEN	Direct Current Electrode Negative
DCEP	Direct Current Electrode Positive
DED	Direct Energy Deposition
DMLS	Direct Metal Laser Sintering
DLF	Directed Light Fabrication
EWW	Effective Wall Width
EBM	Electric Beam Melting
EBF	Electron Beam freeform Fabrication
FZ	Fuzion Zone
GMAW	Gas Metal Arc Welding
GTAW	Gas Tungsten Arc Welding
I	Intersection
LOM	Laminated Object Manufacturing
LC	Laser Consolidation
LENS	Laser Engineered Net Shaping
NI	Non-Intersection
OM	Optical Microscopy
PAW	Plasma Arc Welding
SLM	Selective Laser Melting
SLS	Selective Laser Sintering
SW	Surface Waviness
TWW	Total Wall Width
UC	Ultrasonic Consolidation
WAAM	Wire and Arc Additive Manufacturing

Nomenclature

C_i^{AM}: Cost of rough part made by wire and arc additive manufacturing, £

C_m^{AM}: Cost of machining of wire and arc additive manufactured part, £

C^{AM}: Cost of the final deposited part by wire and arc additive manufacturing, £

C_s: Cost of the starting substrate, £

V_i^{AM}: Deposited volume, m^3

t^D: Deposition time for the WAAM component, h

t^{AM}: Machining time for the WAAM component, h

HR^{AM}: Hourly rate for additive manufacturing cell, £/h

HR^M: Hourly rate for machining cell, £/h

V_s: Initial substrate's volume, m^3

V_f: Final part's volume, m^3

MRR: Material removal rate, kg/h

ρ: Density, kg/ m^3

C_w: Wire cost, £

1 Introduction

1.1 Motivation

Wire and arc additive manufacturing, characterized by depositing metals layer-by-layer with an electric arc and a wire feedstock, has been having a high research interest as it is a direct energy deposition process with high deposition rates, short lead time and with high cost effectiveness, when compared to other AM processes. The materials most commonly investigated for these processes are steel and titanium. However, the need of manufacturing, repairing or replacing components in the aerospace, defence and automotive industry of high strength aluminium alloys made it essential to investigate the use of these alloys on this technology as the traditional forging and post machining of large structures is time consuming, expensive and leads to high wastage of material.

However, aluminium and its alloys are complex metals to weld due to the high thermal conductivity, high susceptibility to porosity and the presence of alumina, which needs to be removed before and during welding. Additionally, aluminium hasn't been extensively studied for additive manufacturing and most scientifically published references on WAAM have characterized mechanically titanium alloys, in particular, Ti-6Al-4V alloy [1].

Wire and arc additive manufacturing has been focusing on simple structures but, to satisfy the industry needs, complex parts need to be researched, as well as the best type of depositions, since the final properties vary considerably when compared to simple structures, as previous studies by Cong *et al.* [2] and Akuno [3] demonstrate.

So far, a small amount of research has been done and published about deposition of AA2319 alloy in WAAM. Up to now, cold metal transfer welding processes have been used successfully to produce simple structures in this metal material. However, alternate current plasma arc welding is the most promising welding process in reduction of porosity and parameter versatility, according to Pinter [4].

However, there's scarce research relative to aluminium deposition with ACPAW (Alternate Current Plasma Arc Welding). In this research project, different deposition strategies for an aerospace part were investigated, using ACPAW on the aluminium alloy referred previously. Therefore, the study on this project will focus on this topic, comparing the porosity, microstructure, microhardness and part efficiency.

1.2 Thesis Objective

The objective of this master thesis was to define the deposition strategy with the best compromise of mechanical properties and overall results for an intersection zone of a specific part of an aircraft component, as showed in Figure 1.

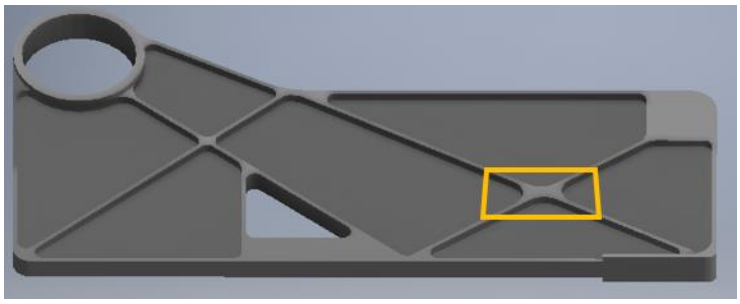

Figure 1: Part of an aircraft component with the zone of interest highlighted.

To achieve the objective, the targets for the project were:

- Deposit aluminium AA2319 filler wire with Alternate Current Plasma Arc Welding (ACPAW) process;
- Implement and validate the wire and arc additive manufacturing software framework currently being developed by Cranfield University;
- Develop and set-up of the deposition parameters and the manufacturing strategy;
- Deposit, analyse and compare different deposition strategies in oscillation paths.

This study was conducted and developed at the Welding Engineering and Laser Processing Centre in Cranfield University, United Kingdom.

1.3 Thesis Structure

This research project is divided in five chapters. Following this initial chapter, chapter 2 contains the literature review, approaching the additive manufacturing (AM) industry with detail in wire and arc additive manufacturing. Moreover,it' current state of the art in the manufacture of large parts, the limitations on depositing aluminium and the two processes suited for its deposition are presented.

The following chapter, 3, exposes how the experimental work was performed, the characteristics of the aluminium wire used, and the methodology employed for the sectioning and preparation of the samples to be analysed and how that analysis was carried out.

Chapter 4 exhibits the results and discussion obtained, including the initial experiments to verify the parameters on the literature and the adaptation to the project in study. Also, a comparison on porosity, microstructure, microhardness, path efficiency, substrate deformation and cost model are conducted to determine which deposition strategy was the best to manufacture the desired part.

In chapter 5, the conclusions from the study at hand are drawn and guidelines' proposal for future work in this subject.

2 Literature Review

2.1 Additive manufacturing

In manufacturing, there are several methods to produce metallic parts, which can be categorized in two groups: the traditional approach, where the part is created with subtractive techniques, e.g. machining, forming, casting, joining, among others, or by additive manufacturing [4].

The first one produces parts by removing material from a bulk/primary stock or sheet metal [5].

On the other hand, and according to ISO/ASTM 52900:2015, “Additive manufacturing is the general term for those technologies that based on a geometrical representation, creates physical objects by successive addition of material” [6].

AM produces (near-) net shape components by adding layers of material on top of a base plate/substrate with each layer being a cross-section of a computer-aided design (CAD) project. The resulting part is an approximation of the data given, as illustrated in Figure 2 [4, 7].

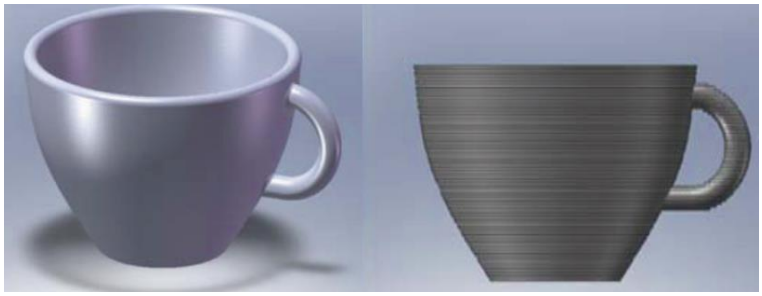

Figure 2: Exemplification of a layered part, constructed through a CAD program [7].

Compared to subtractive manufacturing, this type of technology can produce components with complex geometries, since it does not have the constrains applied to the product design, it consumes less material and therefore having less waste associated. Additionally, parts that needed to be produced separately and then joined with joining processes, per example, may be done through additive manufacturing as a single part [5]. The term AM refers to a broad fabrication processes that include the manufacturing of prototypes, concept parts, tools and functional parts [8].

The recent demands from the automotive, rapid tooling and aerospace industries combined with the possibility to make parts from CAD models (decreasing the development steps), made the AM technology research focused on producing medium to complex shapes and in low quantities in metal alloys that wouldn’t be economically valuable if produced by the alternative manufacturing processes [9].

The additive manufacturing technologies are principally classified as:

- **Direct energy deposition** (DED);
  - Laser consolidation (LC);
  - Directed light fabrication (DLF);
  - Laser engineered net shaping (LENS);
  - Electron beam freeform fabrication (EBF);
  - Wire and arc additive manufacturing (WAAM).
- **Binder jetting**:
  - Powder bed and inkjet 3D printing;
- **Powder bed fusion**;
  - Electron beam melting (EBM);
  - Selective laser sintering (SLS);
  - Selective laser melting (SLM);
  - Direct metal laser sintering (DMLS).
- **Sheet lamination and the processes**:
  - Ultrasonic consolidation (UC);
  - Laminated object manufacturing (LOM) [9].

The AM processes can be classified in terms of the heat source, the material feedstock utilized and the manipulator. The combination of these parameters leads to different AM techniques [4, 10].

Considering the characteristics of the process, the same must be chosen considering their application and the amount of parts produced. For instance, powder-feed/powder-bed process has the capability of producing parts with a high geometrical accuracy with a typical layer thickness of 20-100 μm, with a surface roughness in a range from 9 to 16 μm and a dimensional accuracy of ± 0,05mm. Per contra, the deposition rate of these processes is relatively low (circa 10 g/min) making it unattractive for parts of medium and large dimensions [9, 11]

For wire-feed processes, as the name indicates, a wire is utilized as the supplied material with a 100% efficiency of material used, and the processes can be divided in three sub-categories: arc-welding based, laser-based and electron beam-based. These processes are more environmentaly friendly and don't expose the operatores to the hazardous environment that powder-based processes produce [9]. Additionally, the material rate deposition is higher when compared to the other metallic additive manufacturing processes, enabling a higher workload [12].

Even though AM technologies have enumerous advantages, there are challenges that need to be addressed and forseen. They include the limited amount of materials range used, poor repeatability of the produced parts, lack of standards, poor part accuracy, the "stair-stepping" effect and poor surface finish [8, 11].

This "stair-stepping" effect is present in all of the techniques and is specially evident when there's a construction of round or inclined surfaces [13]. It is caused by the slicement of the horizontal sections and is dependent mainly on the local geometry and the thickness of the layer [14, 15].

2.2 Wire + Arc Additive Manufacturing (WAAM)

Wire-feed additive manufacturing processes are divided into three groups, depending on the energy source: laser, arc welding or electron beam based. The first produces high precision parts but has a very low energy efficiency (2-5%). The latter has a better energy efficiency (15-20%) but depends on a high vacuum environment. Arc welding processes, on the other hand, can reach an efficiency of 90% and the cost, when compared to the other two groups, is lower [11].

WAAM has been having an increase in popularity as it allows the manufacturing of large metal components with high deposition rates, the ability to use welding standard wires and equipment. It is suitable for custom-made and repairing of components, especially in the aerospace industry [16, 17].

This technology has a combination of a metal wire feedstock and an electric arc and its hardware is composed by welding machinery (torches, wire feeders, shielding gas and power sources) and a motion system machine [11], allowing a construction of the part layer by layer (Figure 3-A).

WAAM is aimed for components with low to medium complexity as the size of the deposit bead doesn't allow small or intricate features [4]. A variety of materials are suitable for this type of additive manufacturing technology, such as aluminium, titanium, steel alloys and Inconel®. Thus, for some expensive materials like titanium, the buy-to-fly ratios (ratio of the initial volume/mass by the final volume/mass) in subtractive manufacturing are quite high and the material wastage could be greatly avoided by using WAAM [9].

However, WAAM is a near-net shape process, requiring a final machining process (Figure 3-B) [11] that produces low material waste [18]. Consequently, when designing a CAD file for WAAM, it is necessary to thicken the walls for machining allowance [19].

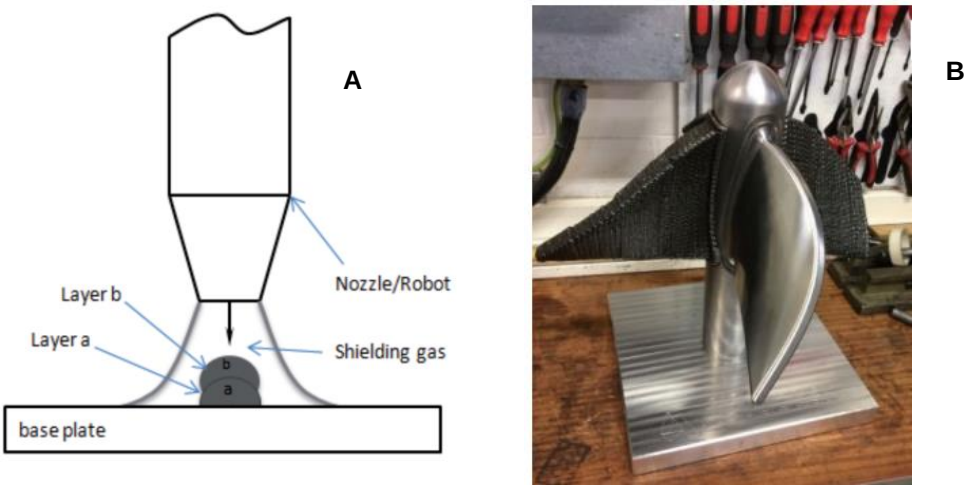

Figure 3: (A) Illustration of a Layer by layer deposition [20]. (B) Example of a WAAM manufactured turbine part, with a machined blade [21].

WAAM is considered a good replacement for traditional manufacturing techniques due to its low equipment and material costs, good structural integrity and high deposition rates (may reach to 6 kg/h [17]). Comparing to other AM processes, WAAM reduces the manufacturing costs and leading times, due to its low buy-to-fly ratios (from 10 to 2 buy-to-fly ratios in some cases) [19].

Some examples of processes included in this category are gas metal arc welding (GMAW), gas tungsten arc welding (GTAW) and plasma arc welding (PAW) as the heating source.

In GMAW, the arc is formed between a coaxial consumable wire electrode and the substrate. there are variants to this process, like cold metal transfer (CMT), which is distinct for having low heat inputs and good material deposition control, due to the dip transfer mode [22, 23].

GTAW and PAW, antithetically, have a non-consumable tungsten electrode to form the arc. Consequently, the feeding system is made externally into the molten pool and onto the substrate [9].

Additionally, the wire-feeding direction, shown in Figure 4, also plays a crucial role, as it influences the transfer of the molten wire and the overall quality of the deposition [9]. The optimum one depends on the material used and on the type of deposition. For example, Syed *et al.* [24] conducted an experiment for a mild steel using a diode laser and concluded that no porosity was found in front feeding but in rear feeding some porosity was observed. However, Xiao *et al*. [25] revealed, for an aluminium alloy with CO_2 laser, that the back-feeding system is more efficient and stable. Furthermore, internal Cranfield University reports state side feeding as the best direction for oscillation path strategies.

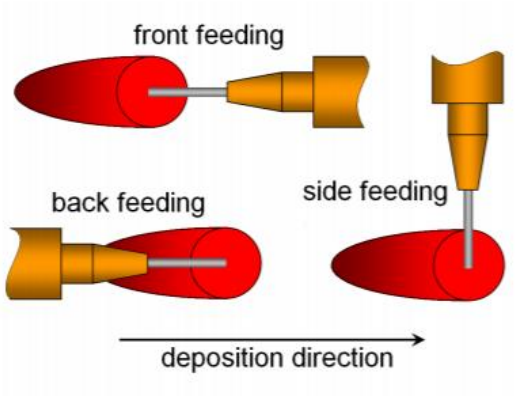

Figure 4: Types of direction of feeding for wire-feed AM technologies [26].

The external feeding system has advantages and limitations. On one side, a coaxial feeding system alloys the path planning programming to be simpler. However, external feeding, there is a control and optimization window over wire feed speed and heat input [9, 27].

Comparing GTAW and PAW, the latter has a retracted electrode which prevents any contamination onto the weld and a narrower arc, induced by the configuration of the weld torch, further explained in 2.2.2 - Plasma arc welding (PAW), which allows less distortion, higher travel speed and higher arc stability [28].

To have a successful deposition, especially when depositing large and complex parts, there are some parameters and part-process planning that need to be controlled and optimized. These are [11]:

- Deposition width;
- Wire diameter;
- Wire feed rate;
- Travel speed;
- Layer thickness;
- Deposition pattern.

2.2.1 Cold Metal Transfer (CMT)

Cold metal transfer process is a GMAW variant and was developed by Fronius®.

The feedstock is fed on a controlled rate from a coil and melted onto a substrate or a previously deposited layer, in a protective atmosphere. However, the electrode and the feedstock are the consumable and the wire feeding system is engaged by retractions in short intervals. [12]

The process has three different phases. The peak current (when a high peak of current causes the ignition of the arc, heating the wire and forming a droplet of melted metal), the background current (decrease of the current to control the amount of material transferred) and the short-circuit phase (the arc voltage goes to zero and the wire is retracted). These three phases go in cycles for the time necessary for the weld [23].

The best CMT variant for welding aluminium, (e.g. AA2319) is CMT Pulse Advanced (CMT-PADV), according to Cong *et al*. [29] and Gu *et al*. [30] due to the low heat-input, low spatter and automatic adjustment of the contact tip to work distance (CTWD), and has been intensively studied for aluminium deposition.

2.2.2 Plasma arc welding (PAW)

Plasma arc welding uses a non-consumable tungsten electrode to produce the weld and has the wire feeding system external to the torch. The torch has a water-cooled copper nozzle in which a tungsten electrode is encircled. This allows the plasma arc to be constricted inside the nozzle and have a shielding gas envelope (Figure 5) [31, 32].

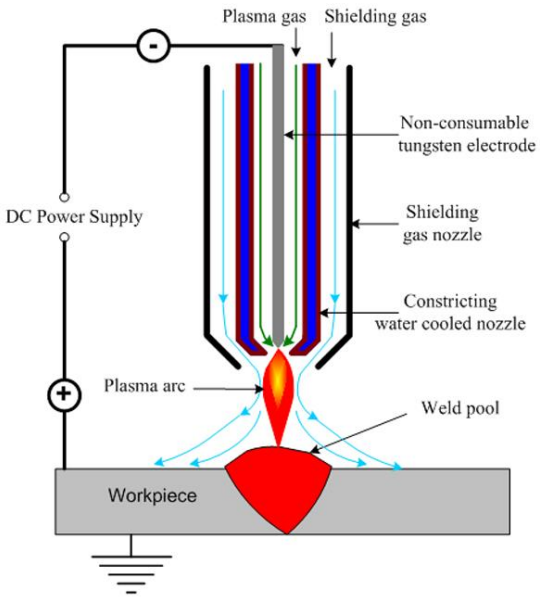

Figure 5 : Plasma arc welding torch configuration [33].

The constriction of the arc results in an increase in energy density and penetration and reduction of the weld bead's width and cross-section area with temperatures that can surpass 1600ºC [34].

The arc is first formed between the copper nozzle and the electrode, with the designation of pilot arc by means of high frequency discharges [32].

This arc is a non-transferred arc with low current. It allows the ionization of the gas and facilitates the start of the transferred plasma arc, as it creates a preferred path for conductance between the workpiece and the electrode [34]. Thus, an expansion in volume due to the high temperatures is observed and is forced through the constrictive nozzle, reaching high velocities. However, the plasma gas flow is insufficient (1-5 L/min) and thereby is required a secondary shielding gas in order to provide adequate shielding effect [31].

As illustrated in Figure 6, the current in the non-transferred mode is flowing from the electrode to the restrictive nozzle and to the power supply. In transferred arc mode, the flow is transferred between the electrode and the workpiece and back to the power supply [34].

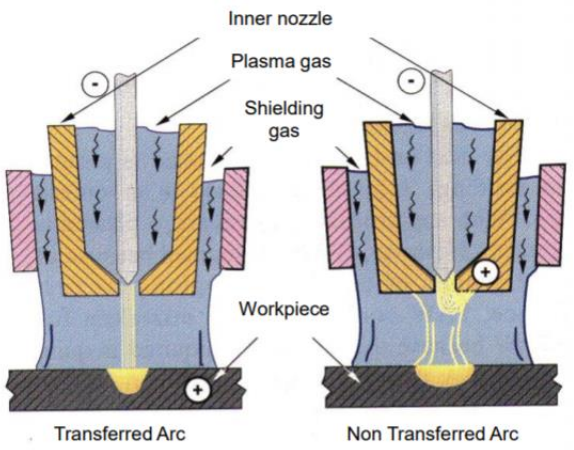

Figure 6 :Transferred and Non-transferred arc welding modes [32].

The gases used in welding of aluminium are usually high purity argon (Ar), helium (He) or a mixture of argon and helium [31].

The external wire feeding system results in an affected consistency on the results. This is due to more parameters that need to be optimized such as the angle of the feeding and the stand-off distance [35].

The welding voltage mainly influences the width of the welds (an increase of voltage increases the bead's width) and the welding current principally affects the penetration depth (higher penetration with higher current). The appropriate current depends on the specific conditions of welding such as the material used, the thickness of the substrate and travel speed [36].

Heat input indicates the energy input to the weld and has a correlation to the microstructure of the weld [37] since it affects the cooling time. Equation (1) allows the calculation of the heat input on arc welding processes where *V* is the voltage used, in volts, *v* is the travel speed, in distance per minute, I is the current used, in amperes and η is the process efficiency. In the case of PAW, the value is 0.6.

$$Heat\ input\ (kJ/mm) = \frac{60 * V * I}{1000 * v}\ \eta \qquad (1)$$

Variable polarity in aluminium

Alternating current results in a fast deterioration of the electrode due to the high current used. However, it is necessary to use this alternate polarity when welding aluminium since it's created a square wave form, which gives a suitable balance between the positive and negative current forms, necessary to melt and remove the oxide layer. The cycle is optimized for the alloy chosen [31]. When PAW utilizes alternate current, it's designation is ACPAW. More detailed information on this topic will be accessible on sub-chapter 2.4.

Advantages of PAW:

- Since the electrode is inside the constricted nozzle, there's less possibility of tungsten inclusions [34];
- The plasma is directional, and the torch can be positioned in different directions [31];
- Low residual stress and distortion [34];
- With the appropriate balance in polarity, the oxide cleaning effect is improved over the processes of gas metal arc welding (GMAW) and gas tungsten arc welding (GTAW) [31].

Disadvantages of PAW:

- Equipment is more complex and costly than other arc processes, such as GTAW;
- Difficult adjustment of the welding parameters due to high installation requirements;
- The nozzle is larger, as it's only cooled by water, contrasting with GTAW which can be cooled by gas, limiting its application to smaller areas [38];
- Welding behaviour is very sensitive to the physical properties of the metal used to deposit and to the parameters (e.g. current) used [28].

2.2.2.1 Comparison between AC PAW and CMT Advance Pulse:

According to a study developed by Pinter [39] on AA2319 aluminium alloy, plasma arc welding produces parts with less porosity and better surface quality. CMT processes induce less heat input into the welds, which may result in more porosity due to the increase of cooling rate, entrapping the gas porosities and may also cause lack of fusion between welds and layers [29, 40].

Both processes provide a good oxide cleaning, necessary to weld/deposit aluminium. However, the polarity in PAW is variable, allowing a bigger adjustment [41]**.** Thus, due to the arc not being produced by a consumable electrode, the stability of the arc is not affected by the quality of the wire [9, 41].

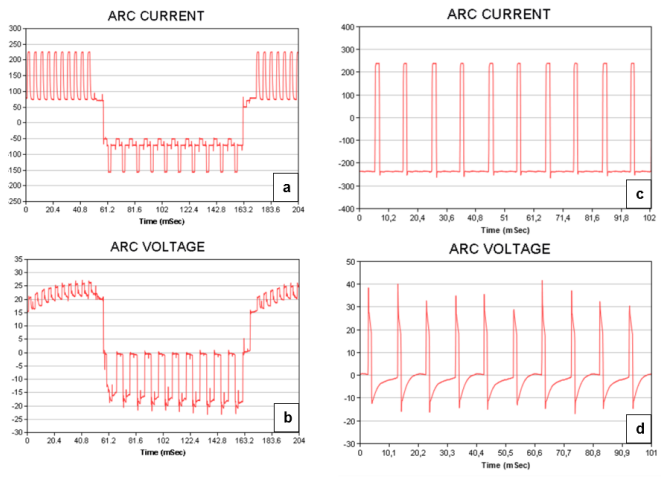

Figure 7 : Pulse cycles on CMT- Advanced Pulse (a) and (b) [39] and on AC Plasma Arc Welding (c) and (d).

2.3 Manufacturing of large parts

WAAM's deposition can be improved by applying more than one welding torch, making it a better choice for producing parts in the industrial sector [42]. Thus, hybrid machining is being investigated [12, 43], to combine a material removal process subsequent to the addition of the metal [42]. However, to produce components with the quality demanded, the deposition should ensure good mechanical properties, so it can outstand the parts made by traditional manufacturing, have defects or flaws below the accepted limit and provide a non-restricted working envelop contrasting with SLM, for example, in order to produce larger components and allow visual inspection and measurements in between layers, and achieve a geometry as near shaped as possible, reducing the surface waviness [11, 9].

This property is defined as the average between the total wall width (TWW – being the maximum width on a section) and the effective wall width (EWW – characterized by being the minimum wall width after machining), indicating the amount of material removed (Figure 8) [44].

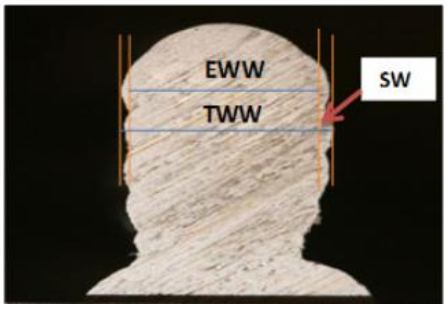

Figure 8 : Surface waviness (SW) measurement [44].

2.3.1.1 Deposition strategies

WAAM, currently, has been more focused in simple structures, as illustrates in Figure 9. However, the engineering components required by the industry are more intricate and a research on these types of structures is necessary [9].

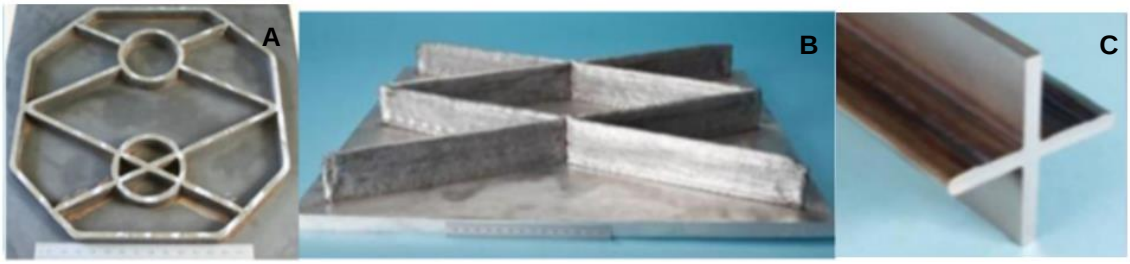

Figure 9: Parts produced by WAAM in (A) carbon steel, (B) aluminium and (C) titanium, with single bead paths [45].

When the wall width required is larger than the one achieved by single deposition, the most used deposition strategies for complex structures is the parallel and the oscillation paths Figure 10. The oscillated has continuum deposition, resulting in a higher heat accumulation, that promotes fusion between the welds and increases the deposition rate and allows the change of wall with by simply changing the oscillation width. However, when compared to parallel paths, the surface roughness is increased [19].

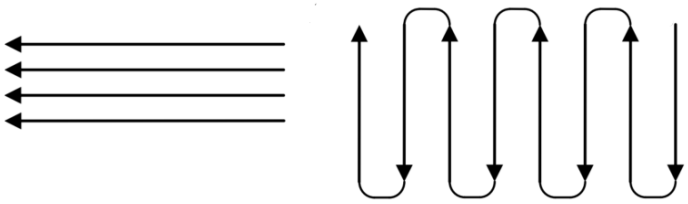

Figure 10: Deposition path strategies. (a) Parallel wall and (b) Oscillated wall strategy [46].

As studied by Foroozmehr [47] and by Nickel *et al*. [48], the deposition patterns play an important role in the thermal history of the deposition and stress distribution. Furthermore, it has been studied that continuous deposition without interpass cooling provides less deformation onto the part since it preheats the substrate. However, a continuous deposition will lead to excessive concentrations of heat, resulting in poor surface finish and dimensional tolerances. Therefore, a compromise between cooling down the deposited layer without causing excessive heating and ensuring a preheating for the next layer should be found. Another method to reduce deformation caused by residual stresses is preheating the substrate before the deposition of the part is started, in order to reduce the thermal cycle temperatures [9]. Cold-work through rolling may also be applied to relieve the residual stresses induced by the thermal cycles, in between layers, and to improve the microstructural properties [49].

2.3.1.2 Accuracy and surface finish

The horizontal slicing of the part's CAD model is made up to a degree of accuracy across the thickness section, in a rectangular shape, not conforming in the vertical axis, resulting in a stair-stepping effect illustrated in Figure 11. This effect will be greater as the thickness of the layer increases. In consequence, the parts made by wire and arc additive manufacturing will have an accuracy lower than other processes (as an example, $\pm$0.2 mm in WAAM vs $\pm$0.04 in Selective Laser Melting) since the layer thickness achievable is also increased (approximately 1.5 mm in WAAM vs 0.02-0.1mm in SLM) [9, 14].

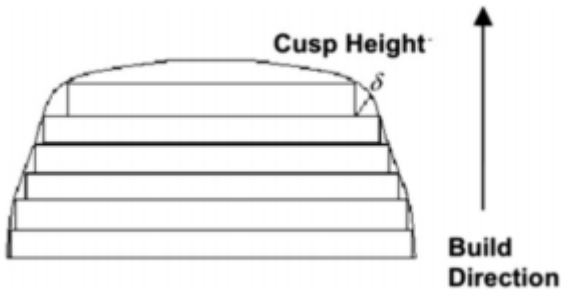

Figure 11 : Stair-stepping effect representation [9].

The weld beads have a parabola shape instead of a rectangular one. The surface of a printed part, as it's an assemble of weld beads side by side and with or without overlap, the surface finish is described as surface roughness. As such, and according to the model represented in Figure 12, if the centre distance, *d,* is smaller than the bead width, *w*, there's going to be an overlap with a decrease of the valley's area. When the area of valley is equal to the overlapping area, the surface will be flat and in an optimal state. However, as the deposition is made layer-by-layer, errors accumulation will lead to an unstable surface [9].

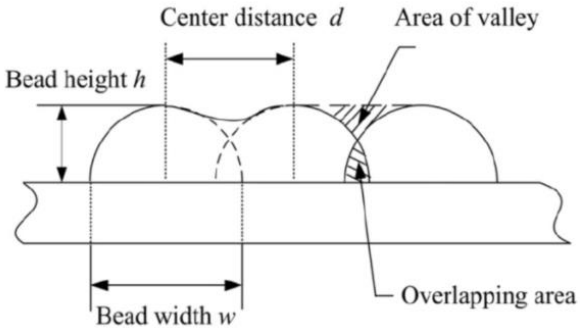

Figure 12 : Overlapping welding beads illustration for parallel and oscillation strategies [50].

A way of trying to compensate the accumulative errors is by planning the paths alternating between the start and finish of the layer deposition (if the path is in a rectangular shape) or by changing the point angle of start and finish (if the section is circular or close figured).

Other accumulative deposition error occurs in the extremities of a weld pass. This phenomenon is due to the thermal influence in the weld bead and may lead to arc instability. At the start, the penetration is lower due to a higher heat sink, resulting in a thicker area. On the other side, at the end of the weld pass, the viscosity is higher, resulting in a slope that, increasing with layers, will become steeper [51]. The way of minimizing this effect is by adjustment of the welding parameters in the start (higher current and travel speed) and end (gradual reduction of current and travel speed) portions of the path to differentiate from the parameters in the middle [9, 52].

Figure 13 : Single wall path [53].

With WAAM, only the first layer is deposited on a flat surface, and the following ones will solidify on top of antecedent layers. Consequently, wetting, surface condition and the spreading behaviour of the weld pool will have a major influence in the surface finish [54].

Microstructure and mechanical properties

When doing additive manufacturing, a specific volume of material is under a complex thermal cycle where there's a high absorption of energy of the heating source, resulting in a fast heating above melting temperature, followed by a rapid solidification due to the small volumes of molten material and localized heat input. Furthermore, when the following layers are added, the material suffers other processes of re-heating and re-cooling.

This leads to a fine-grained microstructure that is dependant of the temperature gradients that, in turn, are influenced by the process parameters and material properties, e.g. the thickness of the layer, energy density, pre-heating temperature, if applicable, and the thermal conductivity of the material.

In addition, microstructure is also affected by the geometry of the part and the direction in which the heat conduction is higher. Thus, if the part if thin, the heat conduction is higher, and the grains will be smaller. However, since this property is not equivalent in all directions, the solidified material will be anisotropic, both in microstructure and mechanical properties (e.g. hardness, tensile strength) [55].

2.4 Aluminium in WAAM

Aluminium is considered a "light alloy" given its low density (2700 kg/m^3 [56]), with high strength to weight ratio, which makes it one of the preferred materials used to reduce the weight of structures or components. It has other important properties for technology such as high electrical and thermal conductivities, recyclability and a high corrosion resistance. It has wide application areas, including aerospace and automotive industries [57, 58].

Regardless of the properties and applications, aluminium is difficult to weld due to its porosity formation, retention of the oxide film, high thermal expansion coefficient and high probability of solidification cracking [42]. However, applying a process with appropriate oxide cleaning, heat treatment or a process of interlayer rolling may mitigate the limitations of the aluminium alloys [42] and is being currently studied by researchers.

2.4.1 Material properties

The excellent corrosion resistance found in aluminium is due to its instantaneously formed protective oxide film, alumina (Al_2O_3). However, in welding, this layer needs to be accounted for as its melting point is 1400 degrees Celsius above the aluminium's melting point (approximately 2050ºC vs 650 ºC) [59, 31].

The additive manufacturing market as a gap in the suitable number of aluminium alloys to weld, since this metal is easy to be machined and the parts have a low cost when compared to titanium, for example. Also, some alloys are difficult to be welded. An example is the 7xxx series, which have volatile elements, such as Zn, that lead to porosity, splatter and turbulent melt pools. On the other hand, the thermally induced stresses are reduced due to the high thermal conductivity of aluminium, also allowing higher processing speeds [55].

Its high thermal conductivity results in high solidification rates, which affect the microstructure. It normally presents itself as cellular, columnar dendritic and equiaxed dendritic, as illustrated in Figure 14 . The columnar dendritic, inclusions and dendritic solidification interface can act as pore sites [29].

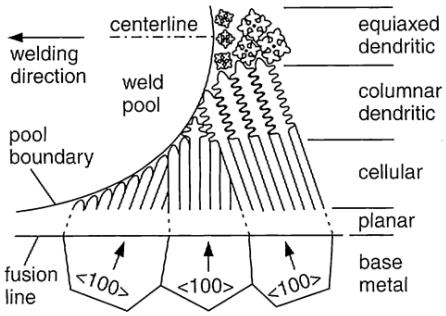

Figure 14 : Microstructure formation in the welded metal [60]

Metallurgical challenges:

Porosity

This defect results from the entrapment of gas dissolved in the molten weld metal when it solidifies, forming bubbles. The size range can vary between micro-pores and coarse pores, that may reach 4mm in diameter [31]. However, for pore diameters ranging between 50-100 µm, preferred crack propagation sites will be created on the pores [61].

When producing a part with aluminium, porosity will be inherent. Depending on the process, wire quality and external operations, this effect can be significantly reduced and eliminated [11].

As solidification is taking place, the small pores will ascend and may combine with other pores, creating larger ones [29].

- **Porosity due to hydrogen**

Aluminium alloys are highly prone to hydrogen gas absorption, due to the high solubility of this element on the molten phase contrasting with the low solubility in the solidified state. The result is the formation of bubbles during cooling, in the solid-liquid interface and, if unable to escape to the melt surface, the solidified alloy will incorporate the gas porosity. Thus, if the cooling rate is high, the diffusion of the hydrogen is unfavourable as it decreases the diffusion time.

Additionally, a higher welding speed will increase the solidification rate of the melt pool, resulting in more, but smaller pores [58, 62, 31].

Even with gas shielding, hydrogen can be present if the substrate or filler material have water, grease, oxides or other contaminants on their surface.

However, previous studies [62] in laser welded aluminium joints indicated that only a percentage (60%-80%) of the porosity gas was hydrogen, whereas the other sources of porosity are different gas elements entrapment or caused by turbulent flow of the welds [58].

The composition of the alloy has a major influence in the porosity by hydrogen. Aluminium alloys with a high content of copper and silicon have a adverse effect since it lowers the solubility of hydrogen in the melt pool and augments the absorption of hydrogen. Magnesium, on the other hand, has the antithesis effect [31].

- **Porosity resulting from turbulent flow on the surface**

The entrapment of the gases may also be related to the turbulent flow in the weld pool. The defects may be an outcome of shielding gas, air or metal vapour [58].

- **Quality of the feeding wire**

An adequate and high-quality wire choice is necessary in WAAM technologies. In fact, the feedstock will have an influence on the corrosion resistance, liquidus and solidus temperatures, microstructure, mechanical properties and porosity. Additionally, the wires may contain defects (e.g. impurities, supersaturated hydrogen) that will have a negative effect on the welds [63, 31]. A visual comparison between different wire surfaces and single bead depositions using nominally similar wires are shown in Figure 15 and on Figure 16, respectively. Some elements found in commercial wires such as Ti and Si are added to form oxides with oxygen and float to the surface of the weld pool, forming slags that will not interfere with the final weld quality [54].

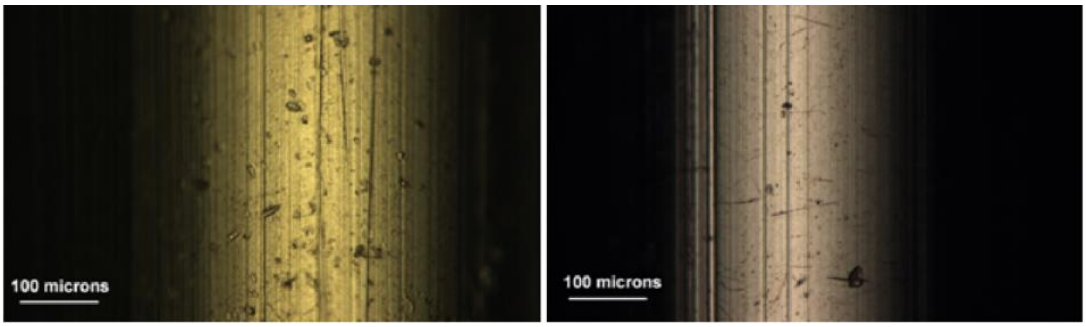

Figure 15: Comparison of two wire surfaces [63].

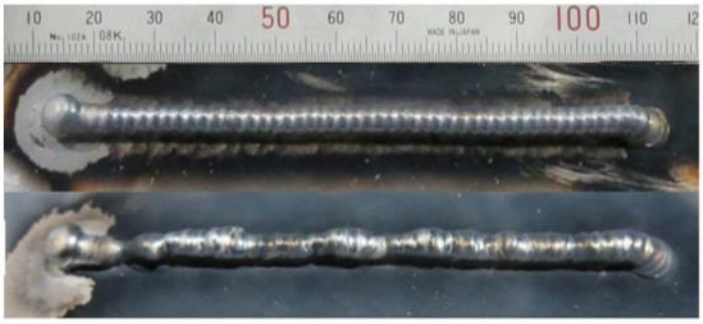

Figure 16: Deposition of single beads using different wires by Cold Metal Transfer – PADV process (adapted) [63].

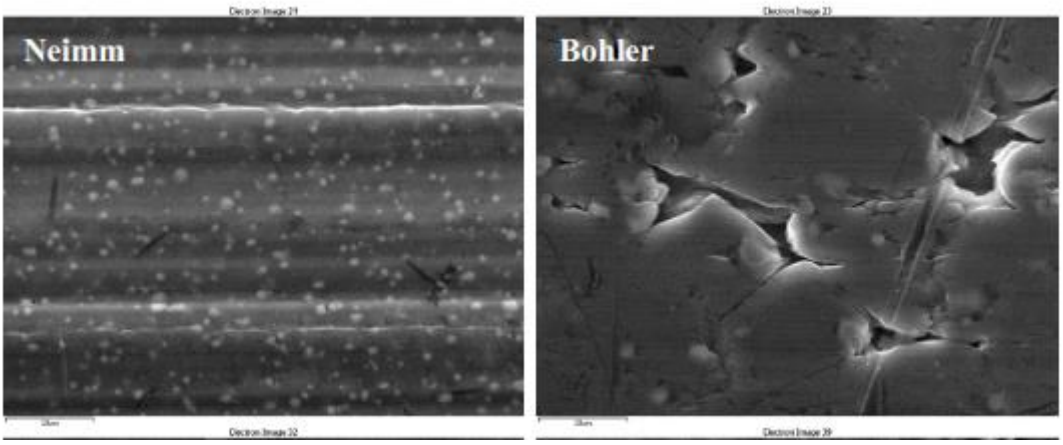

Figure 17 : Aluminium alloy 2319 wire surface from two different welding wire manufacturers in a magnification of 150 times [39].

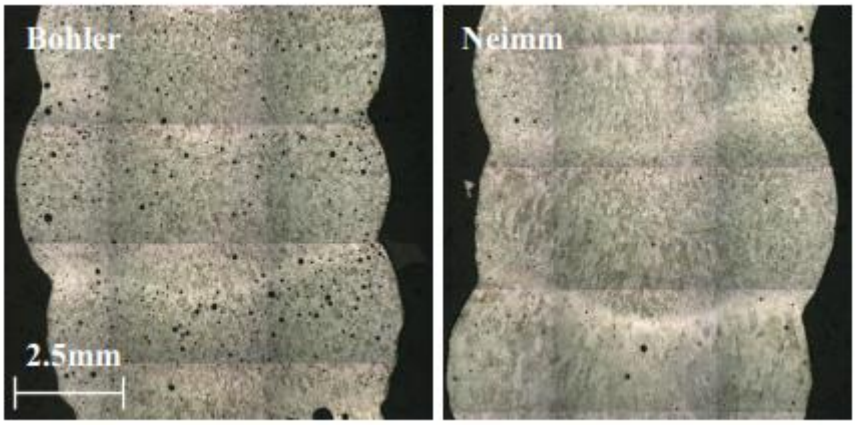

Figure 18 : Effect on porosity by using nominally wires (2319 aluminium alloy) from two different manufacturers using CMT advance pulse process [39].

Oxide inclusions and Oxide cleaning

The oxide inclusions may be originated by imperfect shielding, by oxides resulting from the reactions of the metal with the impure shielding gas, by inaccurate aluminium oxide cleaning or due to the magnesium content.

When an aluminium alloy contains this element in its composition, different oxides may be originated. For example, when the alloy contains more than 0,005 wt.% of magnesium, $MgO.Al_2O_3$ spinel is formed and, when there's a presence of more than 2 wt.%, MgO is formed [58].

As stated previously, aluminium has an oxide layer at its surface which unable its use in most of the arc processes and requires pre-welding surface treatments. A way to overcome the welding capability is to use a process with variable polarity, employing alternating current (AC) of straight and reverse polarity. The first refers to DCEN (direct current electrode negative), where the electrode is the cathode. Reverse polarity, on the other side, is DCEP (direct current electrode positive), meaning the electrode acts as the anode.

DCEP removes the oxide layer efficiently, known as cleaning effect, by bombarding the surface of the aluminium with anions from the electrode, producing high energy and achieving the breakdown of the oxide bonds, removing the oxide layer. At the same time, electrons from aluminium are transferred to the anodic electrode tip, resulting in the wear of the electrode, as seen in Figure 19. Therefore, a fully DCEP polarity is unadvised and variable polarity with a DCEP duty ratio is adopted for higher efficiency [64]. Figure 20 shows the square wave function of the variable polarity plasma arc welding, in which the duty cycle and amplitude of the waveform can be adjusted [28].

The variable polarity achieved by the AC arc will also reduce the hydrogen content from entering the melt pool, as it creates a stirring effect on the pool with the change in electrode polarity in every cycle, aiding the escape of gases [65].

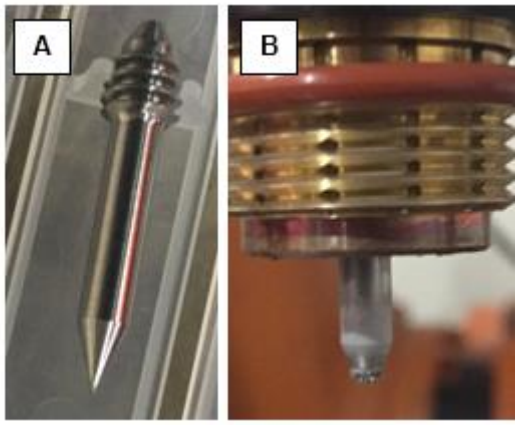

Figure 19 : Tungsten electrodes used for deposition. (A) Before deposition; (B) After deposition in variable polarity;

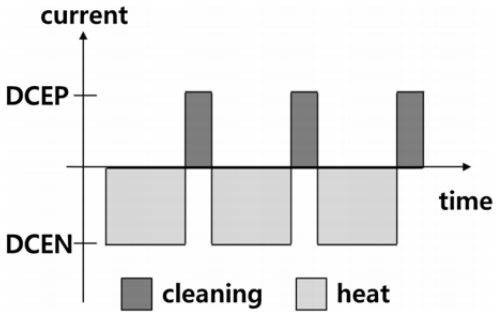

Figure 20 :Illustration on variable polarity duty ratio [64].

Loss of alloying elements

Selective vaporization of low-melting point elements (e.g. Mg, Zn, Li) is caused by high-power welding densities and depends on volume of the weld pool and on the vaporization rate. The decrease of magnesium may reduce precipitation hardening, which affect hardness, corrosion resistance, elongation and yield strength [66].

2.4.2 Aluminium AA 2319

AA 2319 is a heat treatable aluminium-copper alloy, from the 2XXX series. These series have a solid solution of copper in aluminium which increases the strength of the overall material due to the formation of $CuAl_2$ precipitate [31, 67].

The typical usage of this aluminium alloy is for consumable electrode and as filler wire for welding in high strength structural applications and Table 1 lists the main properties of this alloy.

Table 1- Properties of AA2319 [68].

Properties	***Values***
Density	2.83 g/cm^3, at 20ºC
Incipient melting temperature	543ºC
Liquidus temperature	643ºC

2.5 Substrates' Deformation

The wire-feed AM processes induce high heat inputs and high deposition rates. The addition of metal in a previous deposited layer or on the substrate, induces thermal cycles which creates thermal stresses due to the expansion and contraction of the deposited material [42]. This leads to a distortion of the substrate and the part after unclamping, causing losses in tolerances [9].

These stresses are linked to the shrinkage of the material during cooling and are more substantial on the deposition direction. There are some methods that can be used to soothe this problem:

- **Part orientation**: Adjust the orientation of the part before production in order to have shorter tool parts. This strategy results in lower distortion and residual stresses.

- **High pressure rolling between the layers**: This technology induces a vertical load on the layers, resulting in a physical deformation, reducing the residual stresses.

- **Symmetrical construction**: a plane of symmetry, the substrate, will have the deposition performed on both sides, alternated, with the aid of a rotator. With this approach, the residual stresses created on one side will be balanced to the ones produces on the other. Another asset is the heat and time management since, when the layer on side B is being deposited, side A will be able to cool down. However, it may require a redesign to guaranty symmetricity.

- **Building in a back to back approach**: when the part is not symmetrical, when redesign of the part is not possible or when the substrate won't be utilized in the parts produced, the deposition can be accomplished on both sides as well. In this case, the substrate needs to be removed in a following machining process. Figure 21 is an example of this method [11].

- **Heating of substrate uniformly:** as the residual stresses are the result of an unevenly heated body, translated into a non-uniform expansion and contraction of the working material [69], a more uniform deposition may be accomplished to reduce this issue, by layering in a more symmetrical matter. This bullet point was taken into consideration when performing the depositions manufactured in this project.

Figure 21: Side view of a part produced back to back [11].

2.6 Modelling Procedures

2.6.1 WAAM Software

Robotic systems for WAAM processes are able to build large parts. However, the conventional robot programming is generally very time consuming, especially for complex parts/paths [70] , not being a valid option for industrialization of the processes. Therefore, a tool path planning software is necessary to generate path robot codes from CAD models.

A robot path determination program, RUAMROB© was developed by Cranfield university, for the RUAM (Ready-to-Use Additive Layer Manufacturing) project. It was developed in MATLAB 7.1 and contained a layer slicing module and a path program generation module [70]. Per contra, some limitations of this software included the inability to obtain tool paths for complex components and the welding parameters were not included [20].

A more advanced WAAM software is being developed in Cranfield University and aims to tackle the existing gap, for the commercial use of wire and arc additive manufacturing, by developing a framework of automated path planning. This project is still under development, but the ultimate goal is to be able, with the database of processes, materials, complexity of the part and parameters, obtained by Cranfield University, to make WAAM as automated and commercialised as possible.

However, as discussed previously, two major difficulties lie in avoiding defects such as lack of fusion and porosity, as well as maintaining a constant layer height.

To ensure a semi-automatic tooling path planning, five characteristics need to be incorporated by the WAAM software. These are:

1. Build part strategies, to achieve the correct layer height using single bead, parallel and oscillated path strategies. Note that the parameters used will be different from path strategy to path strategy as the thermal effects will be disparate;
2. Process parameter database and interfacing, which will enable the variation of parameters throughout the part deposition in the full 3D part and not only for a single layer. This is crucial, as would ensure a constant layer height and avoid lack of fusion defects;
3. Intelligent partioning, which will do the segmentation of a layer, minimizing the starts and stops and the number of intersections of the layer deposition, avoiding overheating
4. Manufacturing strategy, as for each individual segment after portioning needs to have a building strategy for layer building sequence, define paths for the different segments, etc;
5. Build error checking and correction. This step would be the last one to review for any potential errors and could be made in automatic, semi- automatic or manual mode [71].

Presently, a new software is under development by the same university and enables the integration of any WAAM manipulators and welding equipment with the characteristics presented previously. As stated before, path planning methods have been already studied. However, CAM (Computer-Aided Manufacturing) programmes are mostly used, which provides limitations regarding the development into the machining solution. Consequently, the tool required should create, manipulate paths, visualise, simulate the deposition and post-processes. To achieve this tool, the framework should include a 3D modelling software as well as a coding platform to generate the robot codes and the software implemented was *Rhinoceros3D* and its extension, *Grasshopper,* obtaining two windows of graphical interface. The former, offers the visualisation of the design paths and the manipulators. The latter allows the interaction with the simulation and the generation of paths [72].

Currently, the limitations of the WAAM Software are the manual introduction of segments and parameters into the path planning; the building strategy is limited to oscillation paths, even though this is the most appropriate for complex parts and no automated method for its placement in the segments; a parameters database for materials is yet to be implemented [71].

2.6.2 Cost models

For further interest and upstage in additive manufacturing technologies, it is essential to understand the cost effectiveness. Cost is the driver for decision making in industry and therefore, a cost model followed by a detailed analysis make the tools for the selection of the manufacturing process. As such, it is possible to make a cost effectiveness comparison between AM processes and traditional ones. For industrial applications, the three most significant cost drivers are the materials, the investment and the post-processing [21, 73].

Cunningham, *et al*. [21] developed a cost model which concluded that WAAM processes surpass the other manufacturing and AM technologies, which gives this novel process a promising level of cost effectiveness. Furthermore, since WAAM is still a less mature technology, it is likely that the cost effectiveness of these processes will improve.

Another cost model was created by Martina, *et al.* [4] using volume characteristics such as deposited volume, final volume, volume of the substrate and final substrate volume. With this model, it is possible to compare the WAAM and the traditional machining processes and considers the process used (in this case, AC plasma), the material costs associated and the machine parameters.

The equations for the cost of deposition in by WAAM and for machining are described next:

WAAM cost [4]:

$$C_i^{AM} = V_i^{AM} \rho C_w + t^D HR^{AM} \quad (2)$$

With:

C_i^{AM}: Cost of rough part made by wire and arc additive manufacturing, £;

V_i^{AM}: Deposited volume, m^3;

ρ: Density, kg/ m^3;

C_w: Wire cost, £;

t^D: Deposition time for the WAAM component, h;

HR^{AM}: Hourly rate for additive manufacturing cell, £/h.

Machining cost [4]:

$$C_m^{AM} = t^{AM} HR^M = \frac{(V_i^{AM} + V_s - V_f)\rho}{MRR} HR^M \quad (3)$$

With:

C_m^{AM}: Cost of machining of wire and arc additive manufactured part, £;

t^{AM}: Machining time for the WAAM component, h;

HR^M: Hourly rate for machining cell, £/h;

V_i^{AM}: Deposited volume, m^3;

V_s: Initial substrate's volume, m^3;

V_f: Final part's volume, m^3;

ρ: Density, kg/ m^3;

MRR: Material removal rate, kg/h.

Total cost of the part [4]:

$$C^{AM} = C_s + C_i^{AM} + C_m^{AM} \quad (4)$$

With:

C^{AM}: Cost of the final deposited part by wire and arc additive manufacturing, £;

C_s: Cost of the starting substrate, £;

C_i^{AM}: Cost of rough part made by wire and arc additive manufacturing, £;

C_m^{AM}: Cost of machining of wire and arc additive manufactured part, £

2.7 Summary

From the literature, WAAM is a technology that presents as of highly promising as it provides high deposition rates [9], cost-effective alternatives to traditional manufacturing processes and other AM technologies [9, 74] and low buy-to-fly ratios [19];

However, it presents some challenges, related to the existence of residual stresses due to high heat inputs [9], defects (e.g. distortion, porosity) and further study on the control of bead geometry in necessary. It also has shortage of commercial systems, lack of guidelines and software tools for deposition planning, as well as a demand of high skilled expertise. Furthermore, aluminium is a metal alloy that induces defects. The most challenging are porosity and distortion caused essentially by hydrogen entrapment and residual stresses.

Therefore, building strategies studies are crucial for the development of WAAM in order to take the next step into the industrial sector and to understand the intersections in complex components. Thus, tool-path planning will influence the final product, the efficiency and the mechanical properties [74].

Neto [53] and Chen [75] have studied crossings using CMT-Pulse and T-joints using ACPAW, respectively, in AA2319. However, the analysis of the results was made by visual inspection, and no mechanical properties were evaluated.

AC plasma is a novel technology for aluminium deposition. Chen [75] evaluated the effect of wire feed speed and travel speed on the depositions, simple path crossings and T-joints and Pinter [39] evaluated the impact of the wire quality on porosity and compared the mechanical properties of deposited parts by CMT and ACPAW. They concluded that ACPAW outstands CMT process in terms of flexibility of manipulation, adjustments and porosity formation. Therefore, AC plasma for aluminium deposition should be further studied and, consequently, was the process chosen for this project.

In this context, the present work aims at studying the influence of deposition strategies in WAAM with ACPAW on initial deposition parameters optimization, porosity occurrence, cost of part, microscopy observation, microhardness, path efficiency and substrate deformation to contribute to the industrial implementation of this technology.

3 Material and Methodology

In this experimental work, several and distinct stages had to be considered in order to evaluate the different parameters and variables of the process e.g. the position of the wire feeder and the overlap between the sections.

An overview on the methodology implemented in this work is described in Figure 22.

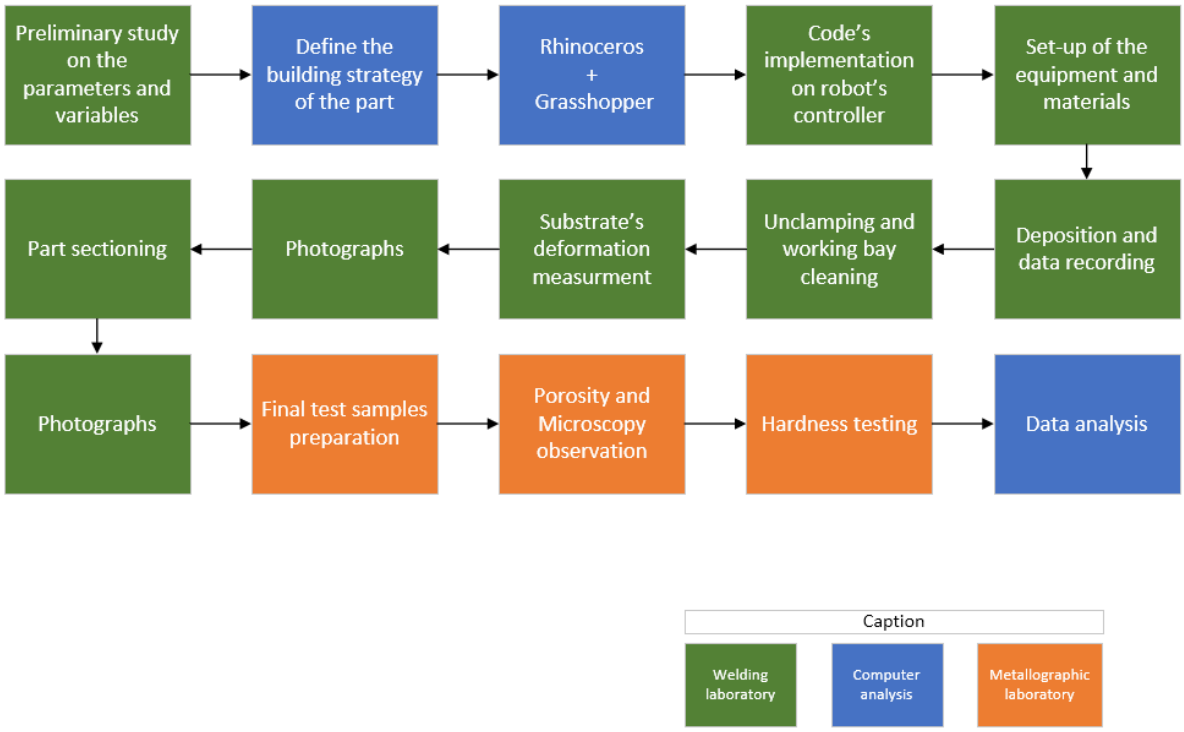

Figure 22: Flow-chart on the methodology implemented on this study.

3.1 Materials

The welding consumable wire used throughout the experimental work was the Böhler-AA2319, with 1.2mm of diameter, as-received.

The substrate material where the geometries were deposited was the aluminium alloy AA6082. The chemical compositions of these metal alloys are available in Table 2.

The substrate plates were cut into the dimension needed (200x200x13 mm^3) to fit the part and ensure enough space for clamping the substrate on the welding table.

Posteriorly, they were subjected to a standard surface preparation according to this order:

1. Washing in warm water with soap to remove the grease and impurities on the surface and air-dried thereafter.
2. Mechanically clean (by linishing) the side where the deposition was being executed with a fine grade disc for aluminium materials to remove the oxide layer.
3. Before deposition, the same surface was final cleaned using acetone.

Table 2 - Chemical composition (wt.%) of the materials used [44, 76].

Material	***Composition***										
	Al	Si	Mg	Cr	Mn	Ti	Cu	Zn	Fe	Zr	Other
Filler AA2319	Balance	≤0.2	≤0.02	-	0.2-0.4	0.1-0.2	5.8-6.8	≤0.1	≤0.3	0.1-0.2	≤0.15
Substrate AA6082	Balance	0.7-1.3	0.6-1.2	<0.25	0.4-1	<0.1	<0.1	0.2	<0.5	-	<0.05

3.2 Equipment Set-up and Deposition

The depositions were accomplished using an alternating current plasma arc welding (ACPAW) system composed by a 6-axes Kuka robot (KR-150), a technical arc wire feeder (ARoboFeed COLD FEED AF40G-taco) and a prototype technical arc AC plasma power source (TECARC OptiArc PLASWELD 400 AC DC HD) on a steel table where the substrates were clamped.

Since the AC plasma welding machine had an uncertain measuring system, an AMV 4000 machine was utilized to monitor and control the welding voltage and current waveforms as well as the wire feed speed for each of the layers.

The set-up of the deposition can be observed in Figure 23.

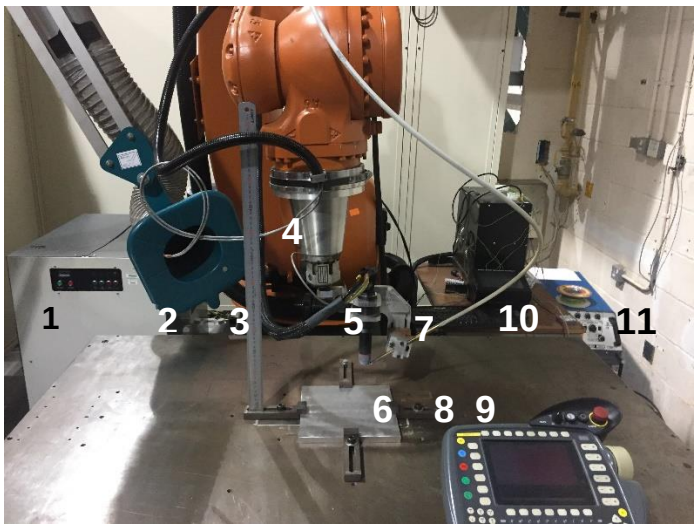

1) System Chiller;
2) Air Exhaust;
3) Ruler;
4) Kuka Robot;
5) Nozzle;
6) Substrate
7) Wire Feeder;
8) Clamps;
9) Robot Controller;
10) AMV4000;
11) Plasma Arc Power Source;

Figure 23: Deposition set-up of the experiments.

3.2.1 Setting of the deposition parameters

Several preliminary experiments were held to determine, optimize and confirm the parameters necessary to build the part in study.

These parameters are influenced by the thickness, width and length of the substrate and the material used. A more detail of the results is described in Chapter 4. The AC current cycle was maintained as 80% DCEN -20%DCEP ratio, as determined by previous studies in Cranfield University as the suited cycle for this feedstock.

To attain a flat surface, a control over the overlap was necessary. In most cases, with oscillation paths parallel to each other, an overlap of 66% was kept constant (value determined previously in a Cranfield University-welding department research [75]). Figure 24 and Equation (5) illustrate the connection between the overlapping area and the centre distance/stepover. The latter being introduced in the WAAM software.

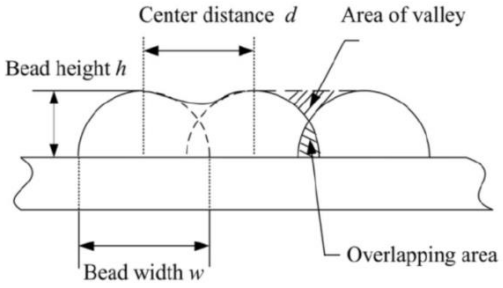

Figure 24: Overlapping welding beads illustration for parallel and oscillation strategies.

$$Overlap\ (\%) = \frac{Centre\ distance, d}{Bead\ with, w} \quad (5)$$

Due to the complexity of the part, the deposition had to be accomplished by combining different sections. The distance between these sections was also studied.

The final parameters used can be observed in Table 3.

Table 3: Parameters for the different deposition strategies.

Parameters	***Values***
Contact Tip to Work Distance	8 mm
Shielding gas flow rate (Ar 99,99%)	20 L/min
Initial current	250 A
Wire feed speed	3.6 m/min
Travel speed	3 mm/s
Centre distance of overlap (in rectangular sections)	3.6 or 4.5mm
Distance between sections	3 mm

3.2.2 Parts' Deposition

The part was deposited with different strategies, using the optimized parameters, as described in 3.2.1.

The successful strategies had the required height (above or close to 20mm) and did not display any visual defect that would influence the part after machining. Those are analysed and compared in section 4.

The layers were produced by depositing oscillated passes, employing side feeding and alternating direction of deposition with each layer.

For each deposited layer, measurements of the layer heights were performed, using a calibrated height gauge in order to obtain an average of the value to insert it the WAAM software.

The interlayer cooling temperature was approximately 70ºC and was measured using a thermometer with a temperature probe.

In Table 4, it is possible to observe the current used for the different layers deposited, for each strategy. The difference in values for the different layers result from the fact that the substrate acts as a heat sink in room temperature, conducting thermal energy by free convection [77]. As such, the initial deposition requires a higher heat input then the subsequent layers. These, per se, have a decreasing heat input, with the increasing distance to the substrate [52]. When the sufficient distance to the substrate is reached, the heat conduction by the substrate is no longer substantial and the heat dissipates mainly through the previous deposited layers, maintaining the current parameter for the subsequent layers.

Deposition strategy 5 was deposited with a wire from a different reel, but from the same manufacturer and composition, due to the shortage of the wire used to deposit S1-S4.

Table 4: Current values for the different layers, depending on the deposition strategy.

Deposition strategies	Current values, A				
	Layer 1	Layer 2	Layer 3	Layer 4	Layer 5
S1	250	230	200	200	200
S2	250	220	190	180	-
S3	250	230	210	210	210
S4	250	230	210	210	210
S5	250	230	210	210	-

3.2.2.1 WAAM software

All depositions were planned using the WAAM software developed in Cranfield University, described in 2.6.1.

The CAD elements, the deposition paths and the robot manipulators' display can be found in Rhinoceros, Figure 25-a. On Grasshopper, Figure 25-b, the user can interact with the setup and create the paths. The path generator will be dependent on a path planning script that allows the user to set the parameters for the deposition [72].

A section of the code for deposition strategy C can be found in Appendix B.

The post-processor will generate a code file to be added to the robot's controller that will be added to initiate the deposition.

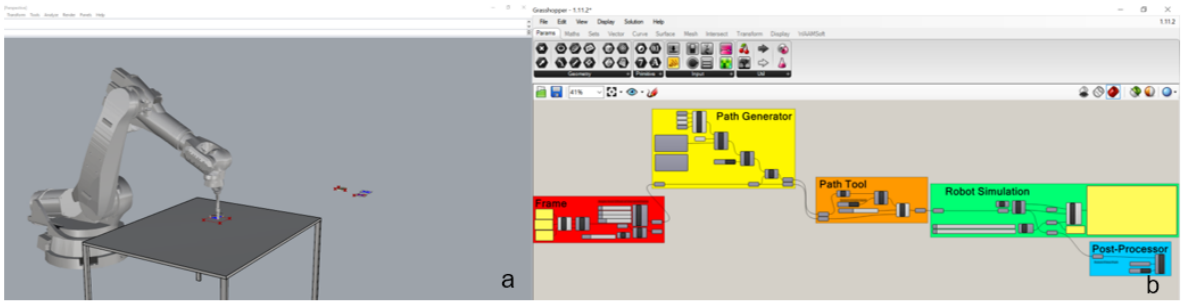

Figure 25: Representation of a path creation on Rhinoceros (a) and Grasshopper (b) using the software developed in Cranfield university.

Deposition images from each strategy will be shown in Chapter 4.

3.3 Samples Preparation

3.3.1 Part sectioning

The zones with more interest were the intersections and the different areas of the part. As such, samples from each deposition strategy were mechanically subdivided as drawn in Figure 26 and Figure 27 presents the C-C sectioning of part 4.

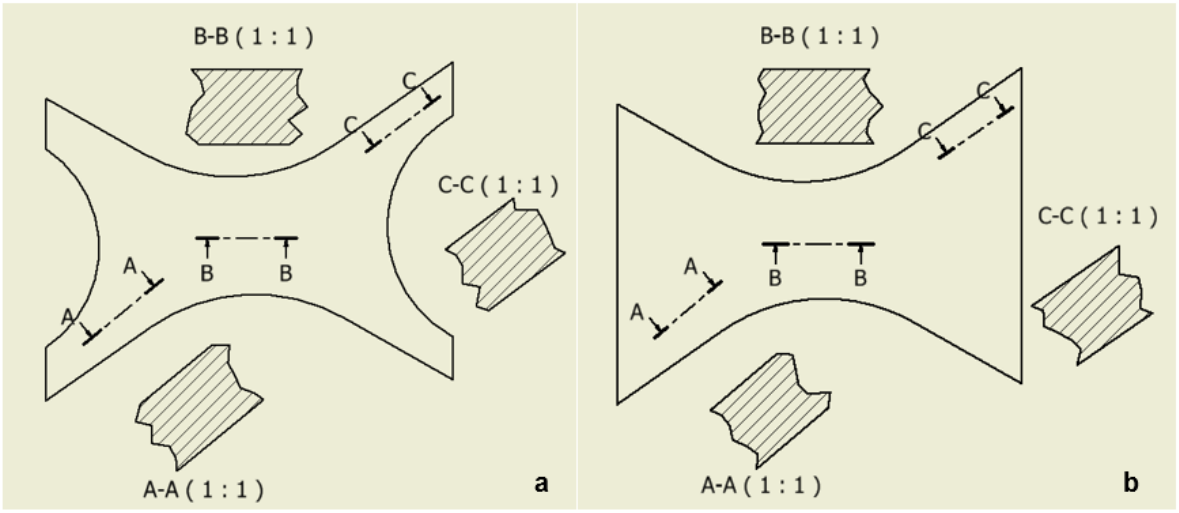

Figure 26: Cut sections for the different deposition strategies. (a) For the strategies 1-4 and (b) for strategy 5.

Figure 27: Wall sectioning of part 4 to achieve the intersection C-C.

3.3.2 Sample preparation

The part was sectioned as mentioned in 3.2.1 in order to get samples for porosity, hardness and microstructure analysis.

Thereupon, they were cold mounted in 40mm cylinder moulds and grinded under flowing water with 240 grit size sandpaper in the opposite surface, so no deviation would interfere with the results.

The grinding and polishing procedure was performed as described in Appendix A.

3.4 Microscopy Observation and Porosity Analysis

The optical microscopy (OM) analysis of the deposited sections was preformed using a Nikon Optishot microscope.

For the porosity analysis and microstructural analysis, optical images were taken of the entire section at a magnification of 2.5 times and stitched together using the software *Image Composite Editor.*

For the porosity analysis, the stitched images were imported to another software, *Image J,* converted into 8-bit images and proceeded into the pore diameter calculation. The final results were presented for comparison in pores fraction area (the analysed area was different from sample to sample) per average diameter of pores, in micrometres.

The analysis of the microstructure was carried out in a similar way as the porosity analysis. Additionally, images were taken with varied magnifications from different zone areas in order to inspect sites of interest.

3.5 Hardness Test

The Vickers microhardness was measured using a Zwick Roell ZHV testing machine. In this test, the load of the diamond indenter was 100g and a dwell time of 15 seconds. The horizontal hardness test was performed in all of the sections. The vertical tests were only executed in the B-B cut, as the results did not vary significantly.

The indentation points were executed as described in Figure 28.

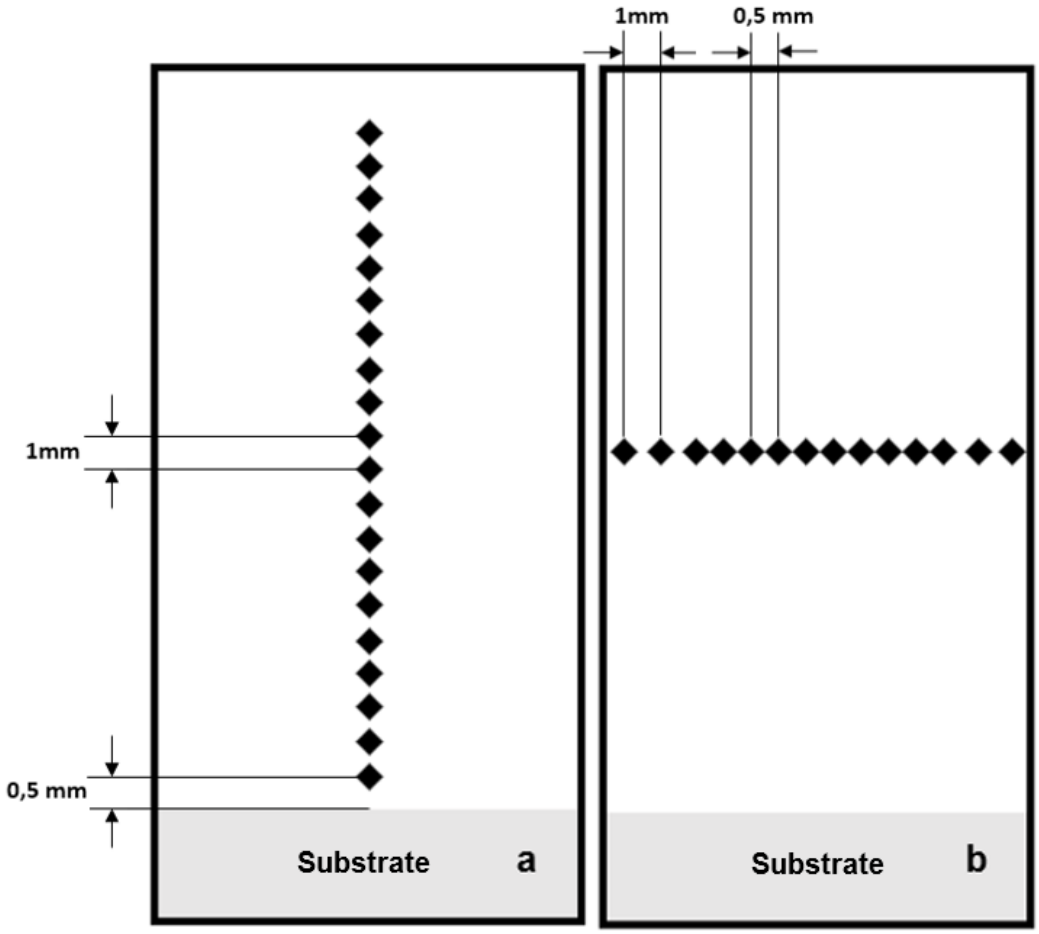

Figure 28 : Hardness test points. a) Vertical measurements and b) horizontal measurements. Figure not to scale.

3.6 Path Efficiency and Substrates Deformation

In WAAM, when it's required a change of deposition paths (different sections), there are two different periods of time to be considered: ARC-On and ARC-Off times.

The first one is considered the productive time, and it occurs when the arc is on, meaning that the material is being deposited and the part/section is being build. On the other hand, the ARC-Off time exists when the process has different sections and accounts the time the robot stops welding a section and moves to another point on the substrate to start a new one. The sum of these two periods makes the total deposition time of building a layer.

The other important period, is the time it takes for the deposited part to be at the temperature required, as explained in 3.2.2 – the cooling time.

The periods were measured by a stop watch, in the same environment characteristics.

The substrates' deformation analysis was carried out using a calibrated height gauge, measuring the difference of the highest point of deformation and the height of the substrate.

3.7 Cost model

A cost comparison between the deposition strategies observed in Figure 26 was held to determine if the added areas (that would have to be removed by a machining operation) in the part shown in Figure 26-b would increase the cost of the part significantly. The calculations were accomplished using the cost model developed by Cranfield University [4], explained in chapter 2.6.2.

The values for the process and material related are tabled. The ones inputted were the volume of the part deposited (V_i^{AM}), volume after machining (V_f), volume of the substrate for deposition (V_s) and volume of the substrate after machining.

4 Results and Analysis

In this section, the effect on how different deposition strategies is presented, with a minimum change in welding parameters, to evaluate the outcome part. It will be carried out by studying the following topics:

- Cost model;
- Microhardness;
- Pore analysis;
- Path efficiency;
- Substrate deformation;

4.1 Considerations

In order to understand the results of this research project and some limitations encountered, some clarifications are needed. These are:

- The average layer height was added to the WAAM software to increment onto the next layer. However, as in AM the deposited layer isn´t regular throughout the surface of the weld, using ACPAW may be a disadvantage as opposed to CMT where there's a compensation of the wire.

- Another advantage of CMT versus ACPAW in this project is the freedom of geometries that may be designed to produce the final part, as the feeding of the wire is made coaxially. This limitation may be observed in Figure 29, as a wire feeder collided with a previously deposited section, due to the oscillation nature of the path planning with side feeding.

- The WAAM software is still under development. As such, some functionalities couldn't be used yet. For example, when the path is long, it would be useful to change the parameters (e.g. travel speed or current intensity) in order to guaranty a stable deposition. Additionally, the method to implement the oscillation path is to use a guideline which is required to go from one side to the other of the section, as visible in Figure 30-a. The strategy in Figure 30-b would be the ideal as the deposition would be made in a non-circular way, guarantying a steady deposition, with less spatter and more automation.

- The plasma arc power source did not provide a precise wire feed speed or current intensity before welding. Therefore, a control with AMV 4000 was necessary in order to have the best control over the results. Additionally, for unknown reasons and with no notice, the controller stopped communicating with the power source and to the robot, causing the robot to stop its movement, while continuing to weld, resulting in structures as visible in Figure 31. When a situation as this occurred, the only way to terminate it was by turning off the power source.

- All the work held so far in aluminium with ACPAW focus on simple structures, in particular with single depositions.

Figure 29 : a) Illustration of the ACPAW torch with the wire feeder and a pre-deposited layer; b) and c) display a practical case of wire feeder collision with section of the part and the wire wastage in the process, respectively.

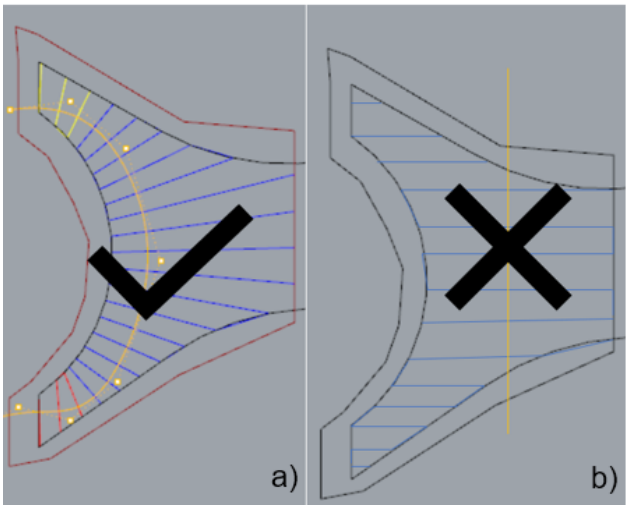

Figure 30 : WAAM software interface. (a) the available method of path planning production; (b) the ideal method of path planning for curved sections. Not possible at the moment.

Figure 31 : Resulting structure after the disconnection of the controller to the robot and power source.

4.2 Set-up of the deposition parameters

To achieve the main goal of this project, which was finding the best deposition strategy for a predesigned part, some steps needed to be accomplished before the depositions took place. These were:

- Adjust the AC Plasma power source, the Kuka robot and the manipulator;
- Validate the WAAM Software for PAW and understand its limitations;
- Verify/optimize the parameters for deposition regarding the ones studied previously.

For extra confidence with the results gathered, AMV 4000 was employed to measure in real time the wire feed speed, the voltage and the amperage.

Figure 32 illustrates the different deposition paths used in the initial set-up of the parameters and Figure 33 shows the initial experiments using those deposition paths. However, it was proven that the parameters will have to be adapted to the dimension of the build plate and the deposition strategy employed. Therefore, the parameters optimized for the simple geometries were not considered.

Figure 32:Deposition paths considering a substrate. (a) Oscillated, (b) parallel and (c) single wall paths.

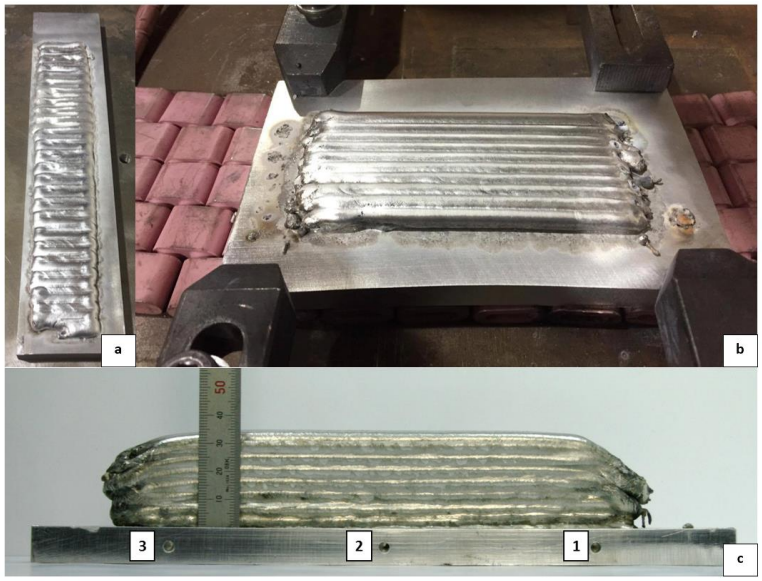

Figure 33: Initial experiments performed by AA2319 as filler wire, AA6082 as the substrate material. (a) Oscillation path;(b) Parallel path and (c) Single wall path. The numeration identifies the voids of thermal couples' insertion.

The preheating of the substrate guaranties a better deposition of the first layer, as it increases the wettability, decreases the residual stresses and consequently, the substrate deformation. This was confirmed by the deposition shown in Figure 33-b and it was also reported by Olari *et al*. [78] and Duarte [79] as the preheating will improve the fluidity of the molten material, decreasing the spatter. However, this solution is not currently adequate for large parts. Since the results of this project will be used to produce the aerospace part presented in Figure 1, preheating was not considered for the depositions in this study. However, a second dry run was performed with the pilot arc, to increase the temperature of the substrate, creating less spatter during the first deposition.

Figure 34 refers to an example of the initial experiments considering the final part and substrate geometry. As stated in chapter 3.2.2, the path strategy chosen was the oscillation path due to the complexity of the part in study. Parallel path could be used, theoretically. However, the efficiency would be considerably lower, the time of production higher and more arc ignitions (starts) and arc extinguishment (stop) would be carried out, decreasing the overall efficiency of the deposition.

Figure 34: Initial experiment, performed by AA2319 as filler wire, AA6082 as the substrate material, to set the parameters in oscillation paths.

Other configuration that needed optimization was the intersection distance, defined by the distance in between two sections, on a layer.

The distances verified were minus one, plus three and plus four millimetres. The latter value had been determined by previous research in Cranfield University to be suited for a T-section with aluminium. **Erro! A origem da referência não foi encontrada.** presents the results of deposition with the distinct distances. The outcomes were:

- For -1mm, there was an accumulation of material in the intersection;
- For 3mm, a flat surface was achieved, and the value employed for the depositions in study.
- For 4mm, scarcity of material in the intersection;

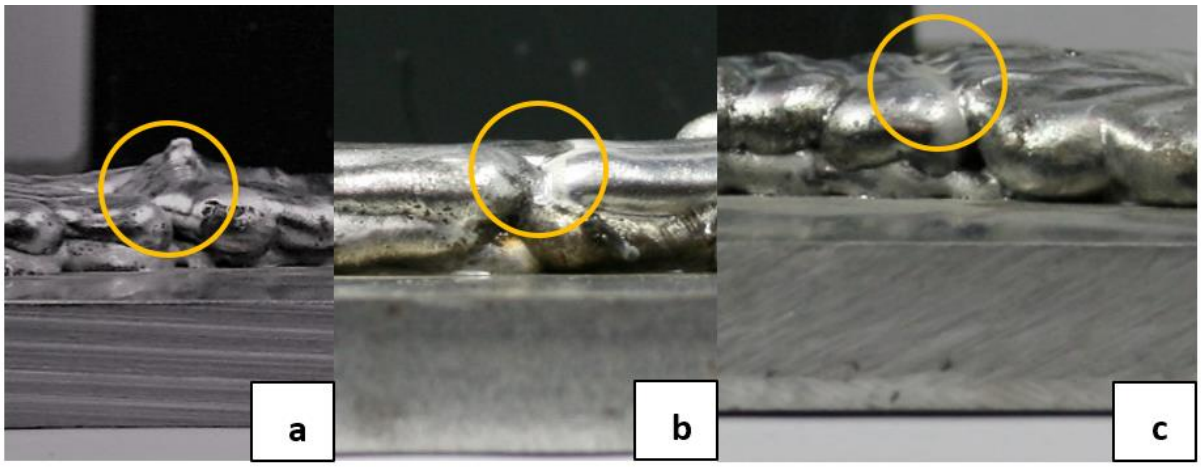

Figure 35: Deposited part with different distance between sections. (a) -1mm; (b) +3mm; (c) +4mm.

The intersections distances -1mm and 4mm, were not suitable for the work to be developed, as a cumulative effect would take place. For -1mm, the chances of the peak to touch the nozzle, inducing a short circuits and material contamination are high; for +4 mm, the depression would be enhanced with the following layers. With +3mm, a flat surface in the intersection is obtained, indicating to be the adequate distance to use.

A stepover of 4.5mm was firstly employed as it had been used by other experimental groups in Cranfield University for parallel walls [53]. The desired cross-section should be similar to the one found in Figure 36 and without lack of fusion defects. However, as seen on Figure 37, lack of fusion defects are visible, due to insufficient overlap, meaning the stepover selected was not the adequate.

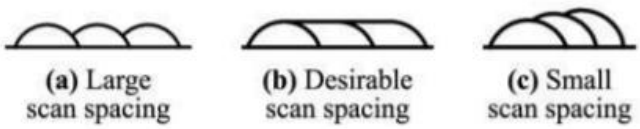

Figure 36 : Overlapping space between the beads [80].

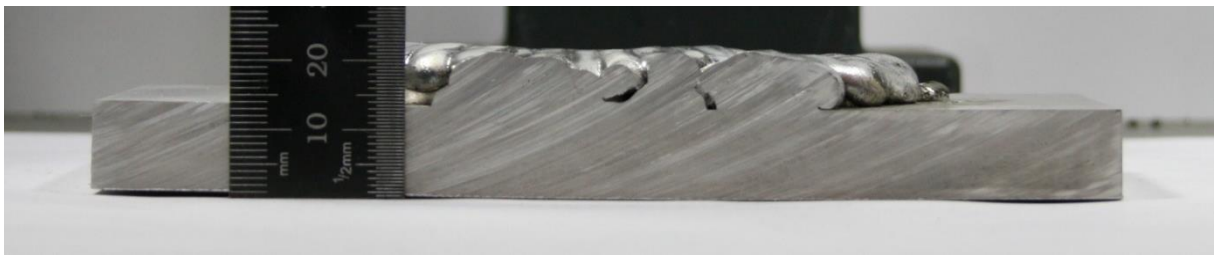

Figure 37 : Profile of the overlapped cross-section with 4,5mm stepover.

On Figure 38, it is possible to observe the surface profile of the overlapped cross-section, with no lack of fusion defects produced in between the oscillation paths. Therefore, the 3,5mm of stepover was employed for the depositions.

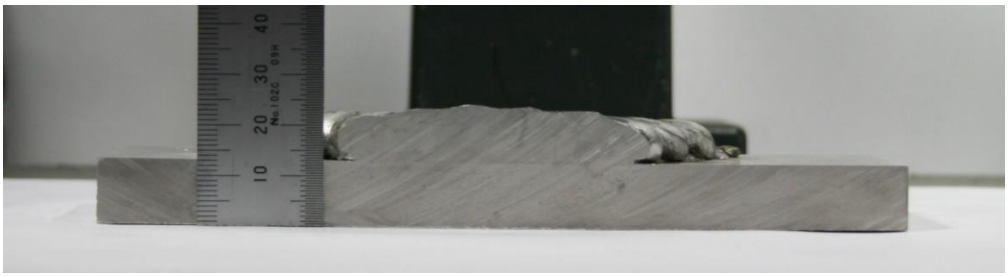

Figure 38 : Profile of the overlapped cross-section with 3,5mm stepover.

4.3 Cost model

The cost model was introduced to compare two geometries: the nearest-shape (Figure 39-A) and the close-shaped geometry (Figure 39-B).

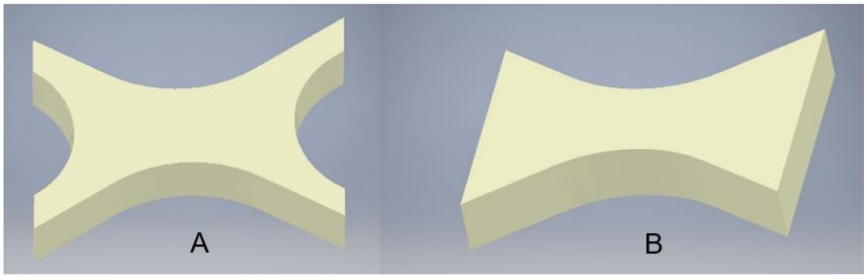

Figure 39 :Geometries considered in this study: (A) Nearest-shape geometry; (B) Closed geometry.

With the close geometry, there's a continuous toolpath with just one start and stop, which reduces the spatter and increases the control of the depositions for, as Venturi, *et al*. states [81], "*arc ignition and stop phases are often the cause of large amount of spatter*". Therefore, the total of starts and stops should be minimum.

The calculations were held using a Cranfield University database which includes the characteristics of the process and materials used for computing the expressions (2), (3) and (4). The data necessary is detailed in Table 5 and considered the CAD file measurements. The volume of the substrate after deposition is not be considered, as it is sacrificial to the final part, in this case. However, it is a necessary input for the database. The cost reduction from building a nearest-shape geometry is 19,3%, which is highly significant.

Table 5 : Cost model inputs and outputs.

Data	***Value Nearest-Shape***	***Value Closed-Shape***
Volume Deposited, V_f^{AM}, m^3	$1.49*10^{-4}$	$1.92*10^{-4}$
Volume of final part, V_f, m^3	$1.04*10^{-4}$	$1.04*10^{-4}$
Volume of the initial substrate, V_S, m^3	$5.2*10^{-4}$	$5.2*10^{-4}$
Volume of substrate after deposition, m^3	0	0
Cost, C^{AM}, £	61	74

4.4 Deposited parts

Five different deposition strategies have been developed and compared. These are shown in Figure 40. All the strategies have been deposited with the same welding parameters, except for particular cases where parameter compensation had to be taken into consideration.

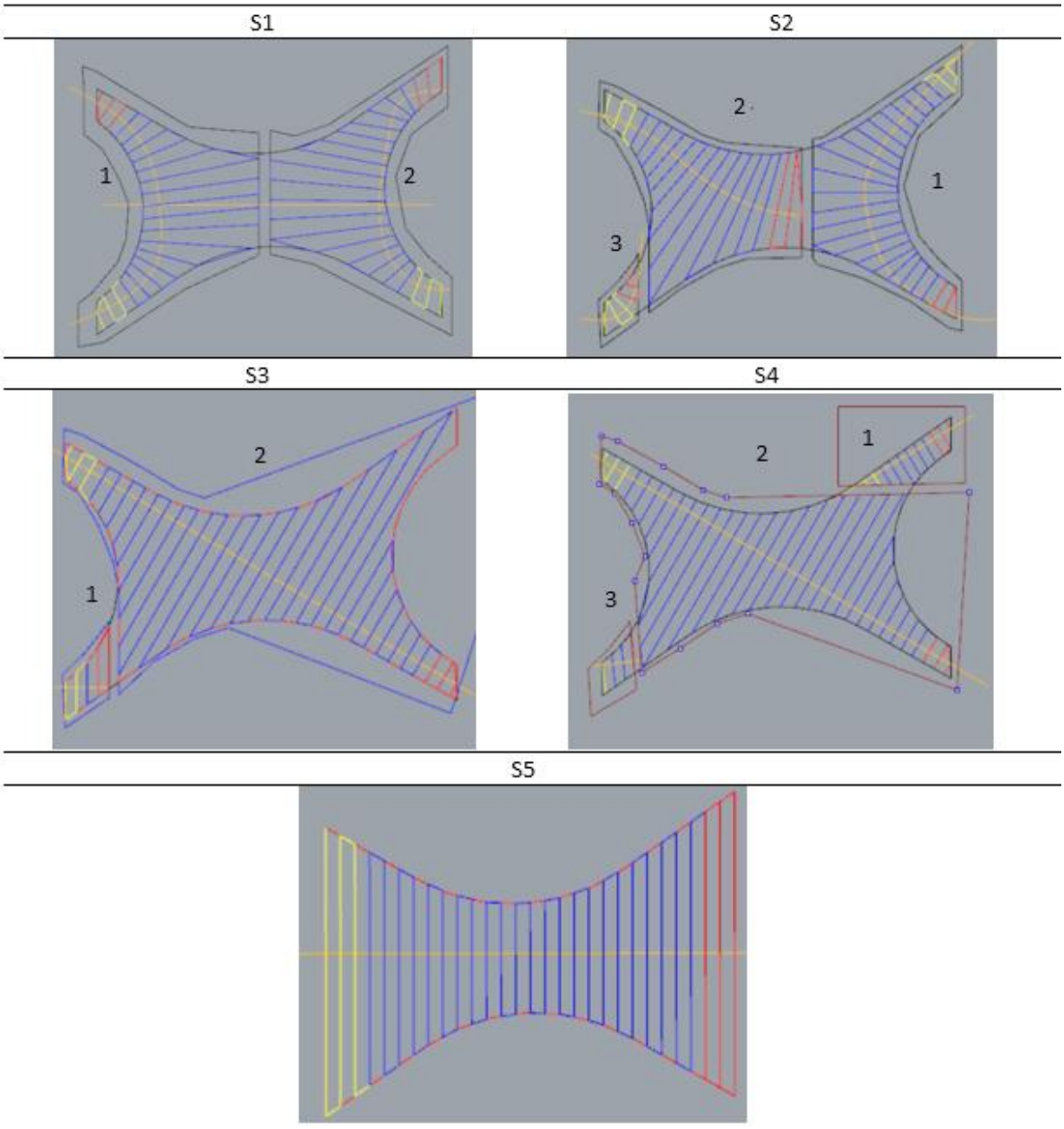

Figure 40 : Deposition strategies considered (S1-S5), numbered by deposition order of the sections.

The deposition, in each section, started in the outmost part of the red zone and finished in the outmost part of the yellow zone, in the numbered order shown in Figure 40. For the following layers, the colours revert, and the deposition starts where it finished last, in order to mitigate the depression, characteristic on the end of deposition.

The parameters used were described in Table 3. For the strategies S1-S4, the centre distance was kept in 3.5mm, as discussed previously in 4.2. However, for S5 the stepover had to be increased to 4.5mm, since the 1st layer height reached an average of 8.16mm, which made the weld pool to touch the nozzle and induce a short-circuit. However, to guaranty enough material deposition without lack of fusion, the travel speed was decreased to 2.5 mm/s and the wire feed speed to 4 m/min.

The deposited parts are presented in Figure 41. The average height of each part is described in Table 6.

Table 6 : Average part height, in milometers and the corresponding number of layers.

Deposition strategies	Average height, mm	Number of layers
S1	19,6	5
S2	13,3	4
S3	23,5	5
S4	23,1	5
S5	23,6	4

S5 has the advantage of guarantying the required height in 4 layers, due to the reduction of TS and increase of WFS.

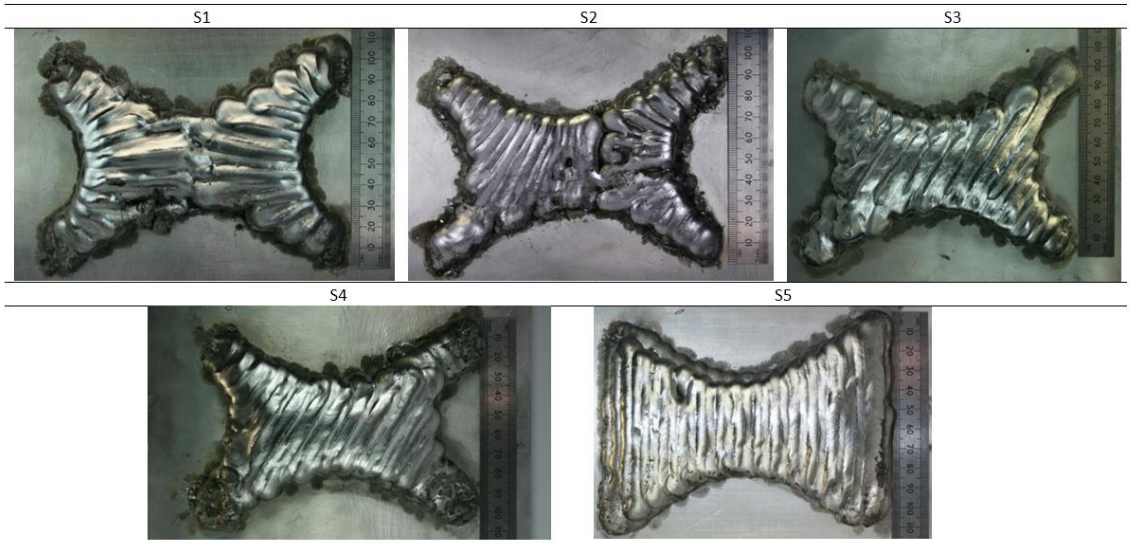

Figure 41 : Deposited parts with AA2319 as feedstock and AA6082 as build plate.

An initial visual inspection was carried out over the five deposition strategies. S2 presented a notorious lack of fusion in the last layer, resulting in the interruption of the deposition, not allowing the part to reach to the minimum of 20mm in height. However, its results for part efficiency were considered. Part S5 also presents a lack of fusion defect in the last layer, a result of the shift of the wire in the melt pool. Due to wire feedstock shortage, a re-do of the part was not possible.

The lack of fusion of S2 in the last layer was caused by the deposition path in section 1. Due to the circularity of the zone, parallel deposition in oscillation was succeeded at the ends but not near the intersection due to a bigger distance on the path near the intersection, when compared to the opposite side. However, the middle part of the section had to be made asymmetrically, as seen in Figure 42.

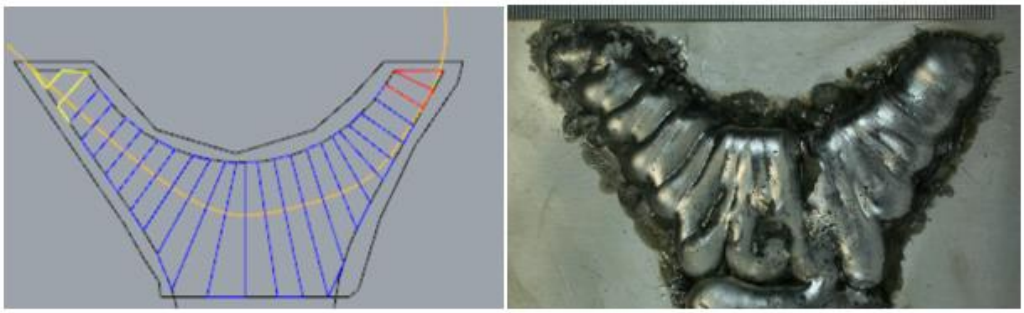

Figure 42 : Deposition strategy and the overall outcome.

The phenomenon was not observed in the previous layers since the decrease of weld current on the forth layer decreased the wall width. This is explained by the wettability of the liquid metal on the solidified layer, as the contact angle decreases, increasing the layer height (confirmed by Graph 1) and decreasing the wall width.

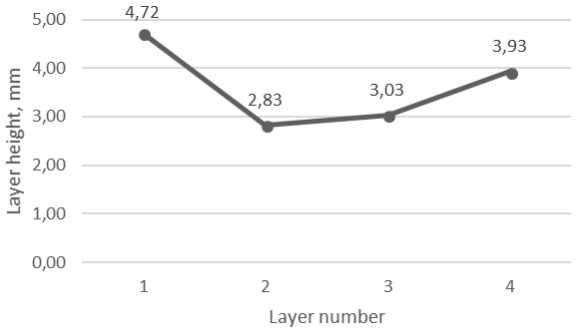

Graph 1 : Average layer height of the S2 layers.

Moreover, in section 2 of the same strategy, the difference in centre distance caused a heterogeneous deposition, that evidenced more material deposited in the closer paths than in the more separate ones, as seen in Figure 44. In fact, the green zone (top) in Figure 44-b had an average layer height of 13,7mm whereas the pink zone (bottom) the average was 10mm. This would lead to extra depositions in order to achieve the desired final height. Based on these two reasons, S2 was excluded from the upcoming results display.

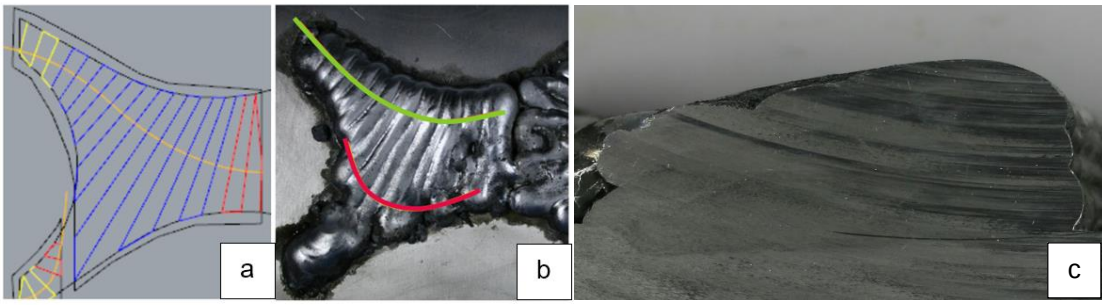

Figure 44 : Section 2 of the deposition strategy S2. (a) Deposition path; (b) deposited part; (c) cross-section.

As the WAAM software did not allow, at the time of the writing of this work, the change of the deposition parameters in a section, the height of the longest edge shows a significant variation in height, as showed in Figure 45. This issue was caused by the long straight movement of the tool-path, resulting in a reduction of temperature (as the torch does not rotate with changing direction) and less heat accumulation, causing a smaller weld pool. This phenomenon was also noticed by Fu *et al*. [82] on a titanium alloy deposition. As it was not a design problem, the results were still considered, even though to reach the ideal height it would require extra depositions. To overcome this issue, another section was created on S4. However, as it was a limitation of the software, S3 results were also considered.

Figure 45 :S3 side view with a focal point on the shorter edge.

For the depositions strategies S1, S3, S4 and S5, measurements of the total wall width (TWW) and the effective wall width (EWW) were carried out as seen in Figure 46 and the results are described in Table 7. Note that the values for S1 were taken in the longitudinal cross-section instead of the transversal cross-section due to the intersection being positioned in the transversal direction.

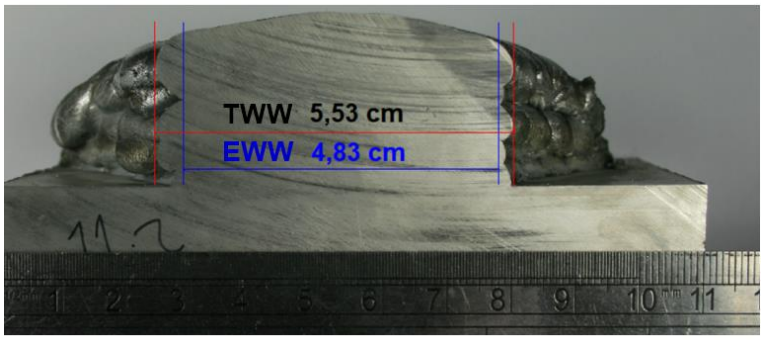

Figure 46 : S4 deposition strategy on the transversal cross-section. Illustration of the measurements of TWW and EWW.

Table 7 : Effective wall width expected after machining and the difference between widths.

Deposition strategies	TWW, cm	EWW, cm	SW, mm
S1	10,03	9,21	4,1
S3	5,06	4,55	2,6
S4	5,53	4,83	3,5
S5	5,32	4,26	5,3

By the analysis of this table, it is visible that the deposition strategy with less material to be removed is deposition S3 whereas the deposition strategy S5 has a higher waste of material. However, when depositing this latter strategy, it was noticed a slight mismatch of the layers by the program, in a layer n+1 matter, caused by the program, which may have affected the results. Previous studies on AA2319 with 1.2mm diameter wire by Ayarkwa *et al*. [44] and by Neto [53] using CMT-PADV process on single bead geometries, displayed the material to be removed ranged between 0,2-0,95 and 0,45-1,2 mm, respectively. Their results were smaller than the ones obtained in this work. However, a straight forward comparison cannot be made, as the path depositions were dissimilar (single walls versus oscillated walls).

4.5 Optical Microscopy Observation and Pore Analysis

4.5.1 Optical Microscopy observation

The microscopy observation between the deposited parts displayed similar grain structures divided by the different areas of deposition. As showed in Figure 47, the lighter areas, also denominated layer bands [83], delimitate the oscillation pattern amongst the layer bands and step advancements.

As described by Cong *et al*. [29], bigger pores will be encountered near the layer bands, as the re-melting of the area will induce the existing micropores to be heterogeneous nucleation sites during solidification. Thus, it is possible to observe on Figure 47-b that the path added last (on the right) has columnar dendritic microstructures near the layer band, perpendicular to the fusion boundary whereas on the other side (left), the structure found is cellular and equiaxed. Due to the complexity of additive manufacturing in terms of re-melting and solidification of the base metal (as substrate or previously deposited layers), the expected microstructure is varied. As stated by Udomphol [84], "*the nucleation and growth of the new grain occurs at the surface of the base metal*". Therefore, the columnar dendritic structures are found near the fusion zone (FZ), with equiaxed dendrites, as Figure 14 illustrated.

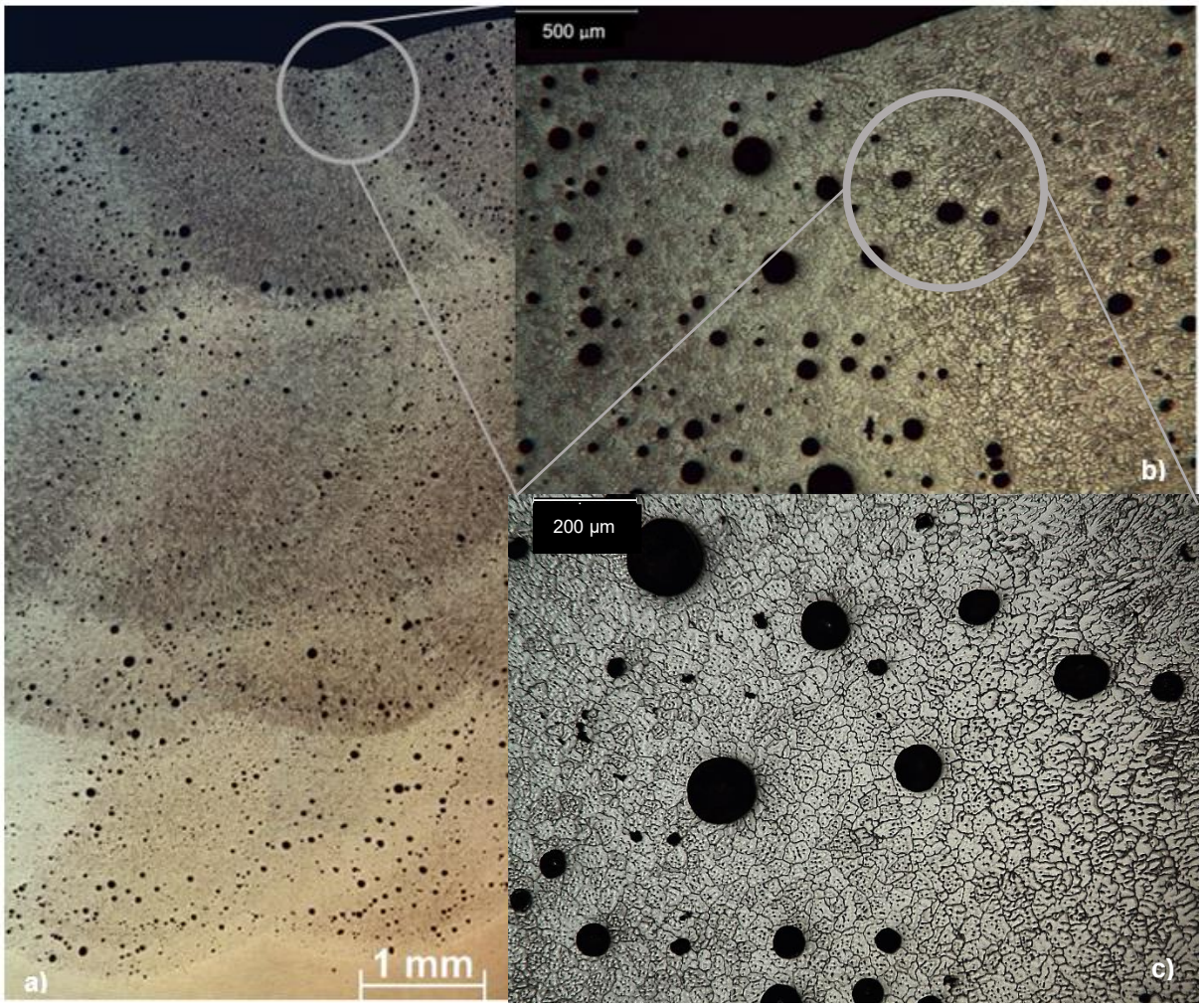

Figure 47 : Microstructure of AA2319 S2 on intersection-1 zone (a) with a 5 times magnification area in detail (b) and with 10 times magnification (c).

The difference in microstructure in the different regions is influenced by the growth rate and the temperature gradient, as it's possible to observe in Figure 48.

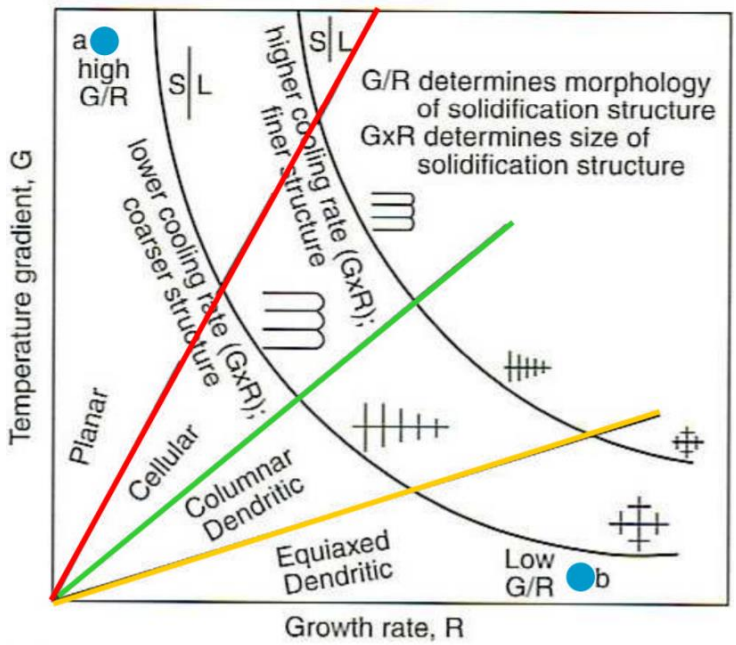

Figure 48 : Influence of the temperature gradient and the growth rate on the microstructure of the weld [84].

As introduced in chapter 2.3.2, the porosity is larger and denser in the dendrite solidification interface and on inclusions, as it works as heterogenic nucleation sites for this type of defect.

This effect is due to the low pressure in the liquid state that allows the small gas pores to float and inter-combine to form larger pores [29].

4.5.2 Pore analyses

Metallographic analyses of the different cross sections were performed to compare the difference in pore size and distribution on the intersections and on the non-intersection areas. As the areas evaluated did not have the same dimensions, the results are presented as average pore diameter, in micrometres, and the fraction area of the pores, in percentage. Pores under 5 µm were not optically visible and, therefore, aren't included in the results and pores in the range of 10-50 µm are considered micro sized pores.

Figure 49 shows the locations of the different cut sections, classifying them as intersections (I) and non-intersections (NI).

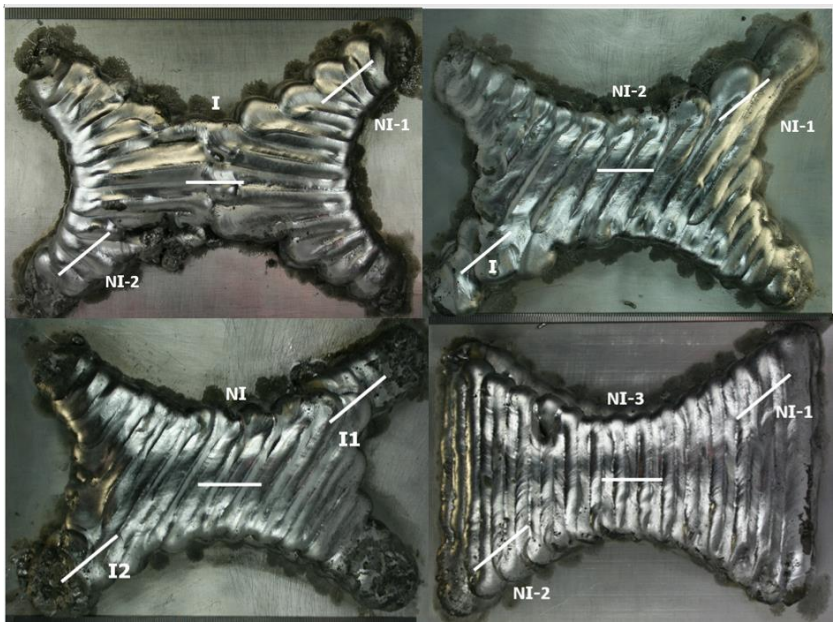

Figure 49 : Naming of the different sections on the S1, S3, S4 and S5 strategies

4.5.2.1 Intersections

The separation of categories between intersection and non-intersection was made to analyse any similarity or dissimilarity between the results.

From Graph 2, it is possible to state that deposition strategies S1 and S3 have similar results regarding the lowest pore size and that intersections from S4 demonstrate similar pore size but different fraction areas. The latter effect may be related to S4-I1 being built first, when there's more instability of the arc.

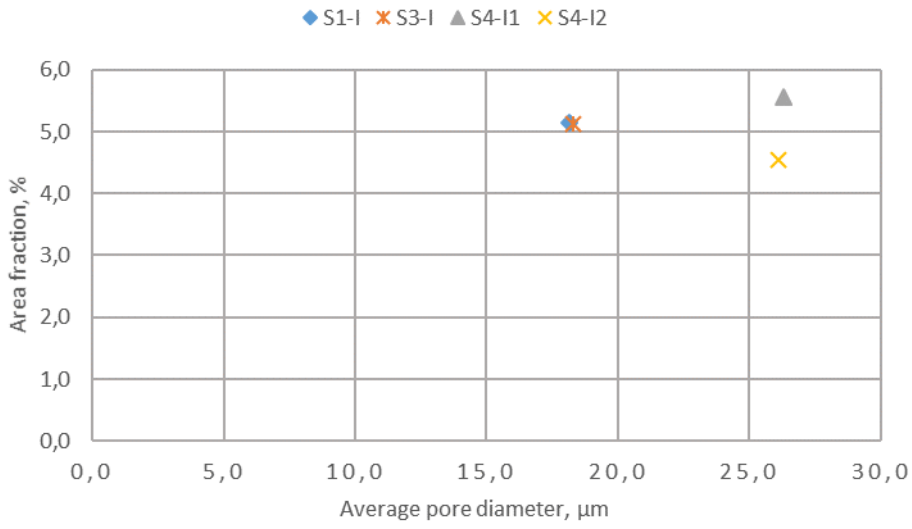

Graph 2 : Pore area fraction by average pore diameter on the intersections.

As stated previously in the literature review, hydrogen entrapment is caused by heterogenous nucleation and is the dominant source of porosity in aluminium. Furthermore, as S4-I1 was the first section to be built for every layer, its cooling rate and temperature gradient was higher, preventing hydrogen to flow onto the surface, being entrapped in the solidified metal.

The area fraction of pores per average diameter on the different sections of the non-intersection areas is displayed on Graph 3. It is possible to state that the higher average pore diameter is 27.7 µm and the lowest is 10.7µm. Furthermore, the obtained values vary in the same deposition strategy, with the highest difference for S3 strategy and smaller variation for S1 strategy. Comparing both strategies, S1 is highly symmetric and the deposition is made more uniformly than for S3, assuring more similarly between the results.

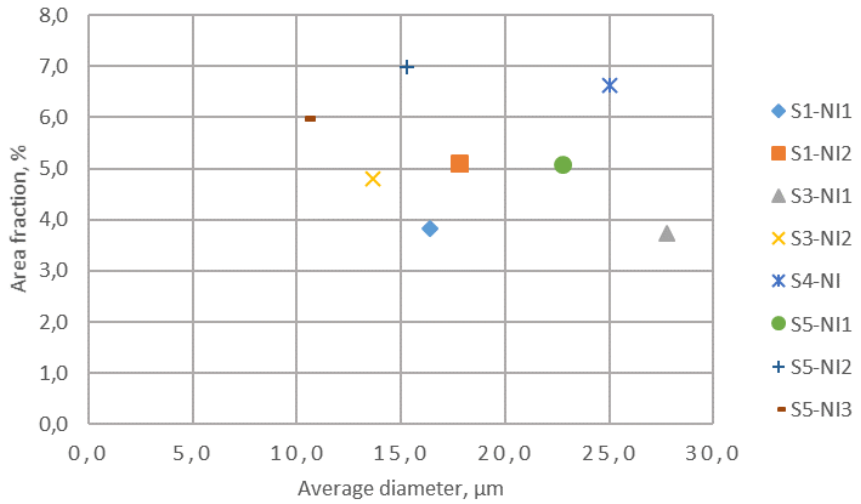

Graph 3 : Pore area fraction by average pore diameter on the non-intersections areas.

S5 displays the highest fraction of area, on average, comparing to the other deposition strategies. The heat flow in this strategy is faster than the other deposition strategies, due to the highest surface area of the deposition (centre distance), resulting in a higher solidification rate, increasing the number of pores (as the pores don't have as much time to reach the surface) but with smaller diameter sizes due to the impediment of flowing to nucleate heterogeneity with other pores, forming larger ones. Furthermore, the wire used for S5 deposition came from a different batch but from the same manufacturer and with the same composition. However, the wire may have had different sources of porosity, which could have resulted in different porosity characteristics.

S4 results are similar to the ones achieved on the intersections. However, it is possible to observe the average diameter on the intersections is higher but with less fraction area then some non-intersections.

As Pinter [39] concluded that the wire quality (that varies with manufacture for nominal wires) has a massive impact on porosity. His results included an observation of porosity decrease when using ACPAW over CMT-PADV, explained by the longer lasting melt pool in ACPAW, allowing the escape of entrapped gases. In the experiments on oscillated walls using ACPAW, pores ranging from 20-85 µm in diameter were observed and the porosity found in this study is also included in that range. Thus, hydrogen entrapment is the main cause of porosity. As this work was performed using the same variety of wire, it's possible to compare only the difference in terms of deposition strategies. It is possible to state that an intersection, for the welding characteristics and parameters used, is not a differentiating characteristic in terms of porosity area fraction nor pore average diameter.

4.6 Microhardness

Microhardness measurements were carried out in order to determine and compare the part's resistance to penetration by plastic deformation in a localized area for the different deposition strategies, as illustrated on Figure 28.

The analyses of the intersections were determined as the most critical ones, when compared to non-intersection areas. Therefore, separate analyses were made to identify the veracity of this premise and conclude if the thermal history of the different zones will lead to distinct properties.

The intersections and non-intersections were named as stated in Figure 49.

4.6.1 Horizontal spacing hardness

Graph 4 presents the microhardness of the samples on the intersections. By its analysis, the hardness values in this area don't present a big variation, except for S4-I2. This hardness increase may be associated with the testing being performed near or on a fusion line, where smaller grain sizes are predominant. For smaller grains, more grain boundaries will be inherent, inducing impediments to the movement of dislocations and increase the deformation resistance of the material.

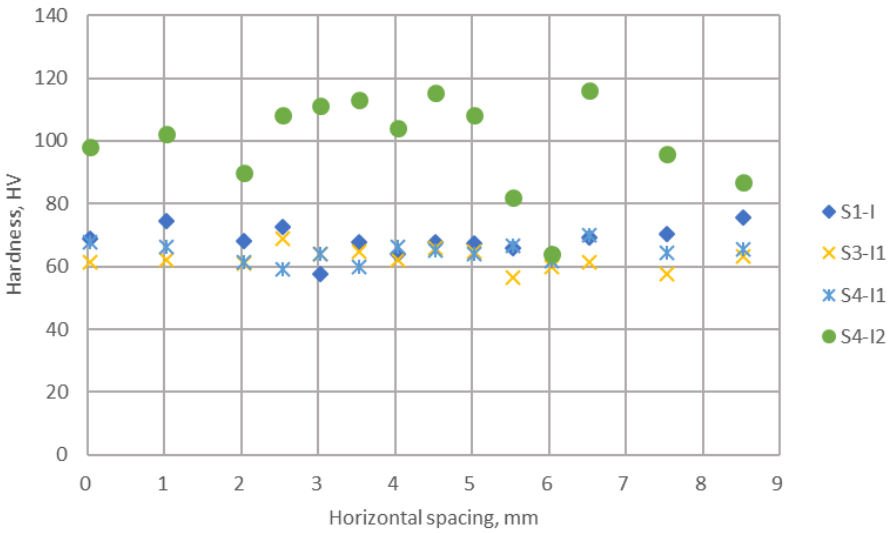

Graph 4 : Hardness comparison of the different deposition strategies on the intersections.

Graph 5 shows the hardness results for the non-intersection areas. It displays a low variation in hardness values between the different sections and in the same measurement. S1-NI2 and S3-NI1 display higher hardness values when compared to the other results, and similar between them. This may have the same explanation as before, with the hardness run test being held on a different section region.

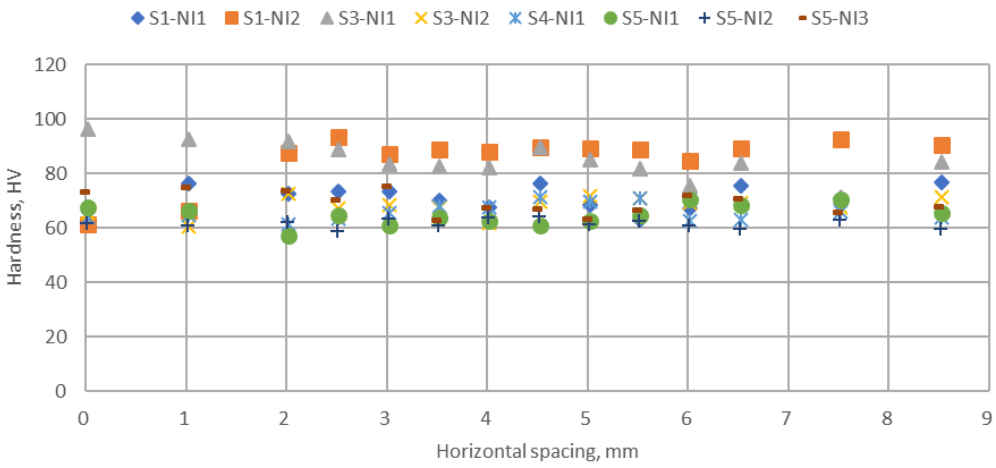

Graph 5 : Hardness comparison of the different deposition strategies on the non-intersections.

4.6.2 Vertical spacing hardness

Graph 6 describes the microhardness on the vertical direction of the B-B sections of the considered deposited parts, where 0 is located at the first indentation starting next to the base plate. It is found that the microhardness values are similar amongst the deposition strategies, with values ranging between 81.2 HV to 63.1 HV for S1, between 76.9 HV to 62 HV for S3, 75.7 HV to 60.8 HV for S4 and 77.9 HV to 62.8 HV for S5. As S1 is characterized by an intersection, differing from the remaining strategies, it is possible to assume that the hardness is independent of this characteristic. Thus, the results change periodically along the vertical axes.

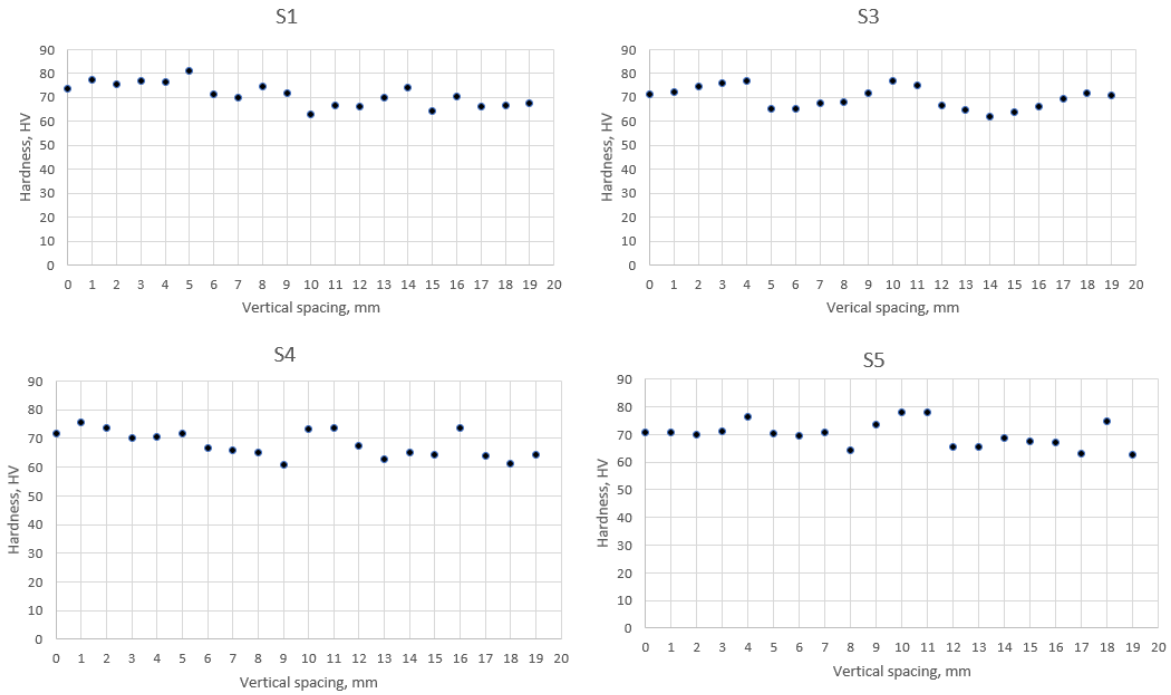

Graph 6 : Microhardness distributions of the S1, S3, S4 and S5 deposition strategies using AA2319 aluminium alloy with vertical distance to bottom spacing.

Cong *et al*. [2] presented similar results by welding the same aluminium alloy in parallel deposition paths with CMT-ADV process but resulting with slight higher microhardness values. This issue may be related to the CMT characteristic of lower heat input when compared with ACPAW, which produces smaller grains, enhancing the microhardness results.

As hardness is the measure of the resistance of the material to plastic deformation, smaller grain sizes will possess a higher number of grain boundaries, as they are obstacles to the dislocations.

4.6.3 Summary

No allotropic phase transformations are found in aluminium. As stated on the microstructure observation chapter (4.5.1) the different deposition strategies on the sections evaluated presented similar microstructures. Therefore, the similarity of the hardness results, as no heat treatment or strengthening techniques were employed, was expected.

Derekar [42] showed in his work a maximum of approximately of 70 HV for an AA2319 alloy and Gu *et al*. [85] presented an average microhardness of 68,3 for CMT-PADV of AA2319 for single wall depositions on vertical measurements, similar to the ones observed in this study.

In horizontal hardness measurements, S5 displayed the lowest average value, as shown in Table 8. It may be related to a decrease of cooling rate, as it has a higher heat input associated.

Gharibshahiyan *et al*. [86] confirmed this theory, by observing that "*any increase in the heat input has an adverse effect on the hardness of welded metals*." And that "high *hardness in the welded zone may be attributed to fine grain size.*".

Table 8 : Average hardness for the different sections.

Deposition strategies	Section	Horizontal Average hardness, HV
S1	NI1	72,3
	NI2	86,5
	I	68,8
S3	NI1	85,8
	NI2	69,0
	I	63,2
S4	NI	66,7
	I1	65,2
	I2	100,45
S5	NI1	65,6
	NI2	62,2
	NI3	70,4

However, as perceived by comparison of the deposition strategies, the strategies with more invariable hardness values are the strategies S1 and S3. Thus, intersection produces hardness values generally lower than the non-intersection ones, contrasting with the vertical hardness results. Moreover, the vertical hardness varies periodically.

4.7 Part Efficiency

4.7.1 Path efficiency

For every path programmed, the efficiency of the useful total time of the deposition (ratio between the arc-on/start and the total time to build a layer) was calculated using (6).

$$Path\ Efficiency = \frac{ARC - On\ time}{Total\ Time} \quad (6)$$

The results on the total time to build a layer in the part are displayed in Graph 7. It is possible to conclude that the total time required to build a layer is minimized in S1 and maximized in S5.

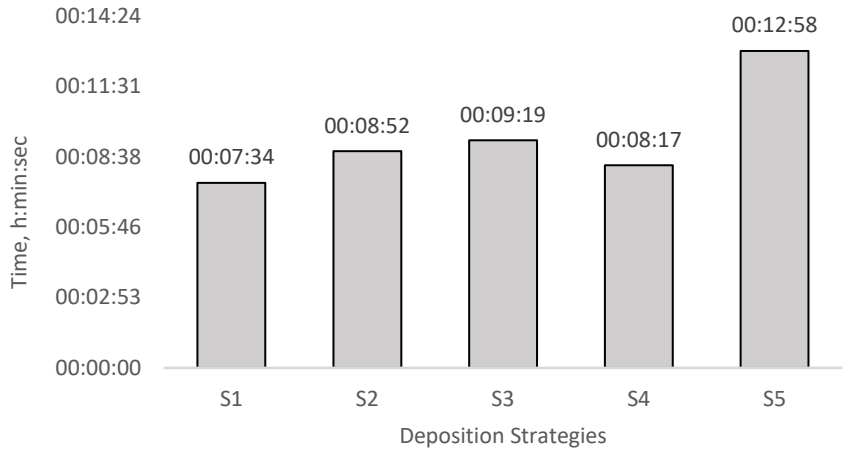

Graph 7 : Results on the total time required to build a layer for each deposition strategy.

On Graph 8, the results on the efficiency of the strategy deposition using equation (6) are displayed and, as expected, the efficiency of S5 is maximum as there's only one section in the strategy. For the nearest-shape deposition strategies, however, the most efficient is S3, closely followed by S1.

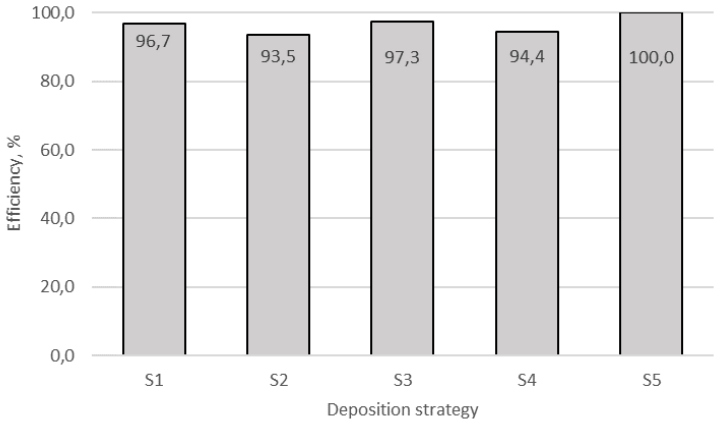

Graph 8 : Results of the efficiency of the different deposition strategies.

4.7.2 Layer heights variation

Layer height measurements were carried out as pictured in Figure 57. The flatness of the surface was analysed by calculating the variance and the standard deviation of the height of the final part. The result is related to the deposition efficiency as it describes how spread out the values are from the mean layer heights.

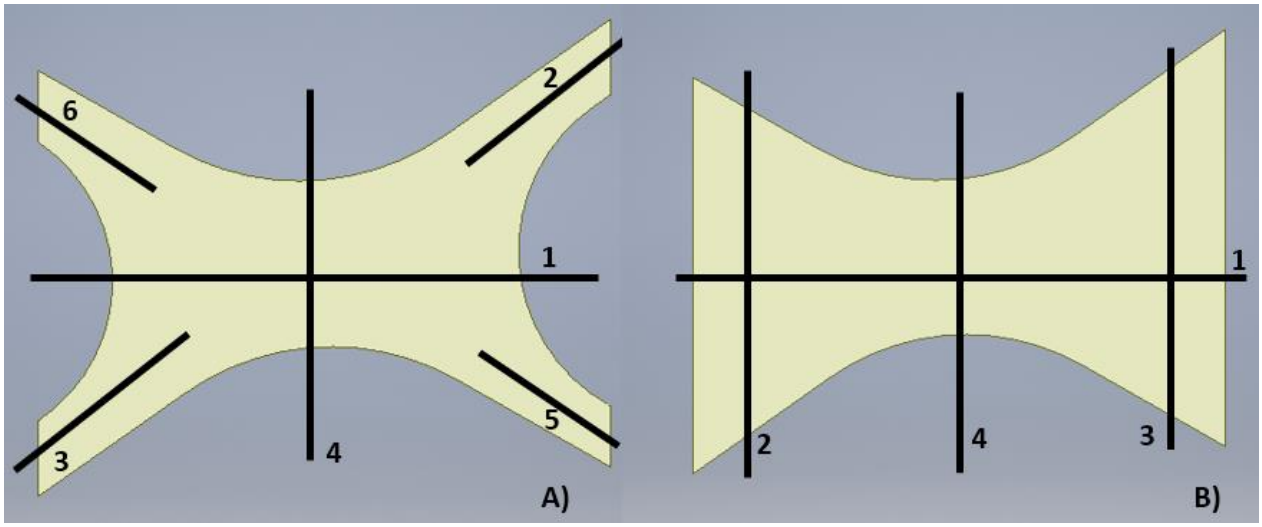

Figure 57: Areas for layer height measurements' analysis. A) for the deposition strategies A to D and B) for the E strategy.

Table 9: Average results of the height measurements on each deposition zone.

Measurement Number	***Deposition Strategy***				
	S1	**S2**	**S3**	**S4**	**S5**
1	20,5	15,2	26,2	26,6	25,2
2	19,8	12,2	23,7	19,5	23,0
3	19,6	12,0	18,6	22,8	22,7
4	19,3	13,6	26,0	25,8	23,7
5	19,5	14,2	23,5	22,2	-
6	18,8	12,8	22,8	21,7	-

The layer heights also indicate the amount of material to be removed in the machining post-processing. If the difference is too high and it does not reach the 20 mm mark, it means another layer of material would be needed to add to ensure that the specifications for the part are fulfilled.

If the distance between the highest point and the lowest points are significant, the effective contact tip to work distance in the different zones will vary, potentially resulting in arc instability and more spatter. So, if the values don't change significantly, the arc stability will be higher and the deposition more efficient.

Through Table 10, it is possible to conclude that the layer heights of S1 (followed by S5) are closer to the mean value, resulting in a smaller deviation in the height of the finished part. Per contra, there's a higher difference, on average, of the data collected and the mean value to the deposition strategies S3 and S4. As stated previously, the CTWD influences the stability of the arc and higher instability may lead to an increase of porosity in the weld. Results gathered on chapter 4.5.2, may be corelated with this statement, as deposition strategies S3 and S4 show a higher average diameter pore size.

Table 10 :Variance and standard deviation of the layer heights of the different deposition strategies.

Deposition strategies	Variance, S^2	Standard deviation, S
S1	1,36	1,16
S3	11,4	3,4
S4	11,9	3,5
S5	3,4	1,8

4.8 Substrate Deformation

The distortions caused by residual stresses need to be analysed and considered on the decision for the best deposition strategy, as the distortion may be detrimental when considering the final dimensional accuracy of the part. Graph 9 shows the substrate deformation for all the deposition strategies considered, including the already ruled out S2. By its analysis it is notorious that the structure with the best performance on the matter is S5, with 1.39 mm of distortion. It may be related to the fact that the deposition is done in the most uniform and symmetric manner. As Ding *et al*. [9] stated and verified, a continuous path with one start and stop is preferred and more advantageous. It is also clear that the deposition pattern and sequence have an important role in the thermal history.

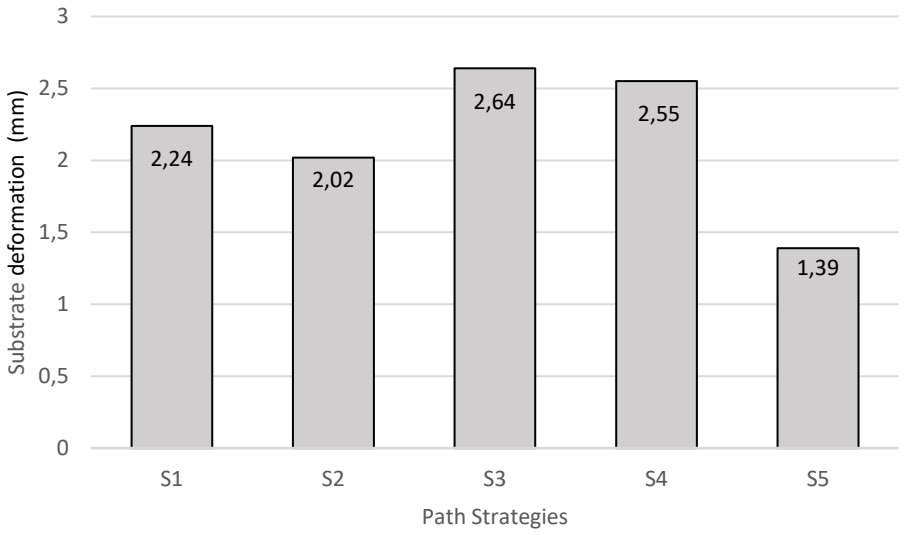

Graph 9 : Substrate deformation results on the different strategies.

4.9 Comparison between the processes

A comparison was made by organizing the data on Table 11. To include the results from the intersections and non-intersections, the average pore diameter was inserted as an average of all the sections.

Table 11 : Overall statement of the characteristics of the various deposition strategies.

Deposition Strategy	***Characteristics***				
	Failures	**Average Pore Diameter, µm**	**Start/Stop**	**Cost estimation, £**	**SW, mm**
S1	No	17.4	2	61	0.41
S2	Yes	-	3		-
S3	No	19.8	2		0.26
S4	No	25.7	3		0.35
S5	No	16.2	1	74	0.53
Deposition Strategy	***Characteristics***				
	Path efficiency, %	**Average part height, cm**	**Height Variance, cm^2**	**Height Standard deviation, cm**	**Substrate deformation, mm**
S1	96.7	19.8	1.36	1.16	2.24
S2	-	-	-	-	-
S3	97.3	23,78	11.4	3.4	2.64
S4	94.4	23.7	11.9	3.5	2.55
S5	100	23.8	3.4	1.8	1.39

The hardness results showed no considerable difference between the different deposition strategies. Therefore, it was not a relevant selection property and chosen not to be included on Table 11 and on the choice of strategy. Table 12 displays the evaluation of the deposition strategies.

Table 12 : Evaluation of the different deposition strategies, considering its characteristics.

Deposition Strategy	***Evaluation***
S1	This deposition strategy excels in the flatness of the overall surface, even though it has an intersection; it produces the second smallest average pore diameter. However, it is not recommended as it produced the smallest part average height, not reaching the desired 20mm and requiring an additional layer deposition.
S2	Unacceptable deposition strategy for this part construction due to deposition failure.
S3	Not suitable deposition strategy, as it induces the highest substrate deformation, has a high average pore diameter and a high standard deviation for part's height.
S4	Not recommended deposition strategy, as it produces the average largest pore diameters; has the lowest path efficiency, higher deviation of values in part height and induces the highest substrate deformation.
S5	Deposition strategy with the average smallest pore diameter; desirable 1 start/stop motion, guarantying a path efficiency of 100%; best deposition rate as only requires 4 layers and reaches the highest part height and assuring the lowest substrate deformation. However, the surface waviness on the sides has the highest values due to the programming mismatch and the deposition cost is almost 20% higher.

5 Conclusions and Future Work

5.1 Conclusions

ACPAW process was successfully employed to produce five deposition strategies of a complex aerospace part using AA2319 filler wire. They were accomplished using the WAAM software currently being developed as well as the optimization of the welding parameters for each strategy. By analysing the characteristics of the depositions, the following conclusions can be taken from this study project:

- Deposition strategies and its parameters are important to guaranty a deposition free of spatter and visual defects;
- Rotation of the torch in circular movements should be avoided, as they require more attention of the operator, decreasing the level of automation;
- The power source should be optimized or replaced, as the interface with the operator does not allow a reliable and accurate parameter control (mainly regarding wire feed speed and amperage). Furthermore, the scale does not show the true value but a range from 1-10 and no integration with programming and the robot can be accomplished. As travel speed is controlled by the robot, this parameter can be included reliably;
- WAAM software still needs some optimization and more control of the deposition parameters, such as changing the travel speed during a straight pass and resolve the mismatch that would occur in some depositions. Program bugs encountered were reported. The path planning should have more freedom, especially when depositing curved areas.
- The microstructure of the different deposition strategies displayed similar grain structures;
- Microhardness values displayed values independent of the deposition strategy and intersection area;
- Intersections study is outmost important, as they influence the arc stability and final characteristics of the constructed parts;

To propose the most suitable deposition strategy, a compromise between the data studied had to be performed. The deposition strategy chosen was S5 as it includes:

- One start/stop motion, producing a path efficiency of 100%, and a continuity of robot-deposition movement when fabricating the final aerospace part;
- Has the best part rate as only requires one less layer to achieve the desired final height;
- Even though the total cost is higher, the distortion of the substrate is the lowest of all the paths considered and the standard deviation of the height of the top surface showed an even surface, resulting in a good arc stability, increasing the process' automation;
- In a manufacturers' perspective, the porosity should be minimised, for strength enhancement. Therefore, the predominant factor choice was the average pore diameter, which revealed to the lowest one for this deposition strategy.

5.2 Future work

As previously stated, the technology used in this study still needs some improvements regarding the power source, the WAAM software and the wire quality used.

Therefore, some future work should be considered, such as:

- Use of reliable ACPAW power source to guaranty repeatable and more accurate results, improving automation;
- Reproduce the proposed deposition strategy with different commercial AA2319 wire on ACPAW and on CMT-PADV and compare the results in terms of porosity and microhardness;
- Further analysis of the heat input on ACPAW and CMT and its correlation with the different characteristics and mechanical properties and interlayer cooling time should be carried out;
- Further deposition with symmetrical construction;
- Replicate hardness and porosity tests to improve statistical significance;
- Further deposition of the other intersections encountered on the aerospace part should be held and optimized.

6 References

[1] S. Chen, Y. Zhang and Z. Feng, Transactions on Intelligent Welding Manufacturing, vol. 1, Springer, 2017.

[2] B. Cong, Z. Qi, B. Qi, H. Sun, G. Zhao and J. Ding, “A Comparative Study of Additively Manufactured Thin Wall and Block Structure with Al-6.3%Cu Alloy Using Cold Metal Transfer Process,” *Applied Sciences,* vol. 7, p. 275, 10 March 2017.

[3] M. P. Akuno, “Characterization of Wire + Arc Additively Manufactured High Strenght Aluminium Alloy Components,” Master of Science Thesis, Cranfield University, 2016/17.

[4] F. Martina and S. Williams, “Wire+arc additive manufacturing vs. traditional machining from solid: a cost comparison,” Cranfield University, 2015.

[5] S. Huang, P. Liu, A. Mokasdar and L. Hou, “Additive manufacturing and its societal impact: a literature review,” *The International Journal of Advanced MAnufacturing Technologies,* pp. 1191-1195, 16 October 2012.

[6] ISO/TC 261, “ISO/ASTM 52900:2015: Additive manufacturing-General principles-Terminology,” 12 2015.

[7] I. Gibson, D. Rosen and B. Strucker, Additive manufacturing technologies - Rapid prototyping to direct digital manufacturing, Springer, 2010, pp. 21-.

[8] N. Guo and M. C. Leu, “Additive manufacturing: technology, applications and research needs,” *Frontiers of Mechanichal Engineer,* pp. 215-243, 2013.

[9] D. Ding, Z. Pan, D. Cuiuri and H. Li, “Wire-feed additive manufacturing of metal components: technologies, developments and future interests,” 23 March 2015.

[10] F. Martina, “Investigation of methods to manipulate geometry, microstructure and mechanichal properties in titanium large scale Wire + Arc additive manufacturing,” PhD Thesis - School of Aerospace, Transport and Manufacturing, Academic year 2013-2014.

[11] S. Williams, F. Martina, A. Addison, J. Ding, G. Pardal and P. Colegrove, “Wire+Arc Additive Manufacturing,” *Materials Science and Technology,* pp. 642-647, 09 February 2016.

[12] J. Prado-Cerqueira, J. Diéguez and A. Camacho, “Preliminary development of a Wire and Arc Additive Manufacturing system (WAAM),” *Procedia Manufacturing,* pp. 895-902, 2017.

[13] E. Yasa, P. Poyraz, E. U. Solakoglu, G. Akbulut and S. Oren, “A study on the stair stepping effect in direct metal laser sintering of a nickel-based superalloy,” *Procedia CIRP 45,* pp. 175-178, 2016.

[14] Y. Y. Yusuf and S. O. Onuh, “Rapid prototyping technology: Applications and benefits for rapid product development,” *Journal of Intelligent Manufacturing,* January 1999.

[15] P. K. Venuvinod and W. Ma, Rapid Prototypin: Laser-based and Other Technologies, New York: Springer Science+Business, 2004.

[16] J. Ding, P. Colegrove, J. Mehnen, S. Ganguly, P. Sequiera Almeida, F. Wang and S. Williams, “Thermo-mechanical analysis of Wire and Arc Additive Layer Manufacturing process on large multi-layer parts,” *Computational Materials Science,* pp. 3315-3322, 2011.

[17] I. Tabernero, A. Paskual, P. Álvarez and A. Suárez, “Study on Arc Welding processes for High Deposition Rate Additive Manufacturing,” *Procedia CIRP,* p. 358 – 362, 2018.

[18] K. Karunakaran, S. Suryakumar, V. Pushpa and S. Akula, “Low cost integration of additive and subtractive processes for hybrid layered manufacturing,” *Robotics and Computer-Integrated Manufacturing ,* pp. 490-499, 210.

[19] J. Ding, F. Martina and S. Wiliams, “Production of large metallic components by additive manifacture-Issues and achievements,” *ResearchGate,* November 2015.

[20] J. Guo, “Feature Based Cost and Carbon Emission Modelling For Wire and Arc Additive Manufacturing,” MSc by Research Thesis, Crafield University, 2011/12.

[21] C. R. Cunningham, S. Wikshaland, F. Xu, K. Kemakolam, A. Shokrani, V. Dhoia and S. Newman, “Cost modelling and sensitivity analysis of wire and arc additive manufacturing.,” *Procedia Manufacturing,* pp. 650-657, 2017.

[22] C. G. Pickin, “Evaluation of cold metal transfer (CMT) process for welding aluminium alloy,” *Science and Technology of Welding and Joining,* vol. 11, 2006.

[23] S. Selvi, A. Vishvaksenan and E. Rajasejar, “Cold metal transfer (CMT) technology - An overview,” *Defence Technology,* pp. 28-44, 2018.

[24] W. U. H. Syed and L. Li, “Effects of wire feeding direction and location in multiple layer diode laser direct metal deposition,” *Applied Surface Science ,* pp. 518-524, 2005.

[25] R. Xiao, K. Chen, T. Zuo, G. Ambrosy and H. Hügel, “Influence of the wire addition direction in CO2 laser welding of aluminum,” *Proceedings of SPIE - The International Society for Optical Engineering ,* p. 4915, September 2002.

[26] A. Heralic, “Monitoring and control of robotized laser metal-wire deposition.,” *Doctoral thesis, Chalmers University of Technology,* 2012.

[27] A. P.M.S. and S. Williams, “Innovative Process Model of Ti-6Al-4V Additive Layer Manufacturing Using Cold Metal Transfer (CMT),” *Proccedings of the 21st Annual International Solid Freeform Fabrication Symposium,* January 2010.

[28] Z. Liu, S. Cui, Z. Luo, C. Zhang, Z. Wang and Y. Zhang, “Plasma arc welding: Process variants and its recent developments of sensing, controlling and modeling,” *Journal of Manufacturing Processes,* pp. 315-327, August 2016.

[29] B. Cong, J. Ding and S. Williams, “Effect of arc mode in cold metal transfer process on porosity of additively manufactured Al-6.3%Cu alloy,” *Advanced Manufacturing Technologies,* pp. 1593-1606, 23 September 2014.

[30] “Wire + Arc Additive Manufacturing of Aluminium,” *25th International Solid Freeform Fabrication Symposium,* pp. 451-458, 2014.

[31] G. Mathers, Welding of Aluminium and its alloys, CRC press, 2002, pp. 10-25.

[32] P. Vilaça, “Plasma Arc Welding,” Materials Joining and NDT, Aalto University, 2015.

[33] Plasma arc welding processes, “TechMiny,” [Online]. Available: http://techminy.com/plasma-arc-welding-process. [Accessed 27 04 2018].

[34] I. Pires and L. Coutinho, “Classes on Plasma Arc Welding,” Instituto Superior Técnico, Lisbon, 2017.

[35] A. Scotti and R. Aparecido dos Reis, “Parameter Optimization of AC Rectangular Wave Outputs for Aluminum Cold Wire GTAW,” *Journal of the Brazilian Society of Mechanical Sciences,* December 1999.

[36] C. Shen, “Application of wire-arc additive manufacturing (WAAM) process in in-situ fabrication of iron aluminide structures,” Doctor of Philosophy thesis, School of Mechanical, Materials, and Mechatronic Engineering, University of Wollongong, 2016.

[37] T. Melfi, “New Code Requirements for Calculating Heat Input,” Lincoln Electric, ASME, 2010.

[38] C. Wu, L. Wang, W. Ren and X. Zhang, “Plasma arc welding: Process, sensing, control and modeling,” *Journal of Manufacturing Processes,* pp. 74-85, 2014.

[39] Z. Pinter, “Study of Aluminium Wire + Arc Additive Manufacturing,” Cranfield University, Master of Science thesis, 2017.

[40] J. Bai, H. Ding, J. Gu, X. Wang and H. Qiu, “Porosity evolution in additively manufactured aluminium alloy during high temperature exposure,” *IOP Conference Series: Materials Science and Engineering,* 2017.

[41] U. Krüger, “TALAT Lecture 4201: Arc Welding Processes: TIG, Plasma Arc, MIG,” 22 October Published on 2009.

[42] K. S. Derekar, “A review of wire arc additive manufacturing and advances in wire arc additive manufacturing of aluminium,” *Materials Science and Technology,* 08 April 2018.

[43] F. Li, S. Chen, J. Shi, H. Tian and Y. Zhao, “Evaluation and Optimization of a Hybrid Manufacturing Process Combining Wire Arc Additive Manufacturing with Milling for the Fabrication of Stiffened Panels,” *Applied Sciences,* 28 November 2017.

[44] K. Ayarkwa, S. Williams and J. Ding, “Investigation of pulse advance cold metal transfer on aluminium wire arc additive manufacturing,” *International Journal of Rapid Manufacturing,* vol. 5, pp. 44-58, 2015.

[45] P. Colegrove and S. Williams, “High deposition rate high quality metal additive manufacture using wire + arc technology,” Cranfield University, 2010.

[46] P. Colegrove, A. McAndrew, J. Ding, F. Martina, P. Kurzynski and S. Williams, “System Architectures for Large Scale Wire + Arc Additive Manufacture,” *10th International Conference on Trends in Welding Research, Japan,* October 2016.

[47] E. Foroozmehr and R. Kovacevic, “Effect of path planning on the laser powder deposition process: thermal and structural evaluation,” *The International Journal of Advanced Manufacturing Technology,* pp. 659-669, 2010.

[48] A. Nickel, D. Barnett and F. Prinz, “Thermal Stresses and Deposition Patterns in Layered Manufacturing,” *Materials Science and Engineering A,* pp. 59-64, 1999.

[49] P. A. Colegrove, H. E. Coules, J. Fairman, F. Martina, T. M. H. Kashoob and L. D. Cozzolino, “Microstructure and residual stress improvement in wire and arc additively manufactured parts through high-pressured rolling,” *J Mater Process Technol,* pp. 1782-1791, 2013.

[50] D. Ding, Z. Pan, D. Cuiuri and H. Li, “A multi-bead overlapping model for robotic wire and arc additive manufacturing (WAAM),” *Robotics and Computer-Integrated Manufacturing,* pp. 101-110, 2015.

[51] Y. Zhang, Y. Chen, L. Pengjiu and A. T. Male, “Weld deposition-based rapid prototyping: a preliminary study,” *Journal of Materials Processing Technology,* p. 347–357, 2003.

[52] F. Martina, J. Mehnen, S. Williams, P. Colegrove and F. Wang, “Investigation of the benefits of plasma deposition for the additive layer,” *Journal of Materials Processing Technology,* pp. 1377-1386, 2012.

[53] L. M. Neto, “Studying the Application of Additive Manufacturing to Large Parts,” MSc Thesis, Instituto Superior Técnico, Lisboa, 2017.

[54] X. Xu, J. Ding, S. D. C. Ganguly and S. Williams, “Oxide accumulation effects on wire + arc layer-by-layer additive manufacture process,” *Journal of Materials Processing Technology,* pp. 739-750, 2018.

[55] D. Herzog, V. Seyda, E. Wycisk and C. Emmelmann, “Additive manufacturing of metals,” *Acta Materialia,* pp. 375-376, 20 July 2016.

[56] Granta Design Limited, “CES EduPack software,” Cambridge.

[57] I. Polmear, Light Alloys - From Traditional Alloys to Nanocrystals, Oxford: Elsevier, 2006.

[58] X. Cao, W. Wallace, J.-P. Immarigeon and C. Poon, “Research and Progress in Laser Welding of Wrought Aluminum Alloys. II. Metallurgical Microstructures, Defects, and Mechanical Properties,” *MATERIALS AND MANUFACTURING PROCESSES,* vol. Vol.18, pp. 23-49, 2003.

[59] R. Sarrafi and R. Kovacevic, “Cathodic Cleaning of Oxides from Aluminum Surface by Variable-Polarity Arc,” *Supplement to the Welding Journal,* pp. 1-10, January 2010.

[60] K. Pal and S. K. Pal, “Effect of Pulse Parameters on Weld Quality in Pulsed Gas Metal Arc Welding: A Review,” *Journal of Materials Engineering and Performance,* pp. 918-931, 2011.

[61] J. Gu, J. Ding, S. Williams, H. Gu, P. Ma and Y. Zhai, “The effect of inter-layer cold working and post-deposition heat treatment on porosity in additively manufactured aluminum alloys,” *Journal of Materials Processing Technology,* pp. 26-34, 2016.

[62] M. Kutsuna and Q. Yan, “Study on porosity formation in laser welds of aluminum (Report 2)—mechanism of porosity formation by hydrogen magnesium.,” *Welding Internaional,* vol. 13, 1999.

[63] J. Gu, J. Ding, B. Cong, J. Bai, H. W. S. Gu and Y. Zhai, “The Influence of Wire Properties on the Quality and Performance of Wire+Arc Additive Manufactured Aluminium Parts,” *Advanced Materials Research,* vol. 1081, pp. 210-214, 2015.

[64] J. Cho, J. Lee and S. Bae, “Heat input analysis of variable polarity arc welding of aluminium,” *International Journal of Manufacturing Technologies,* pp. 1273-1280, 2015.

[65] R. Kumar, U. Dilthey, D. Dwivedi and P. Ghosh, “Thin sheet welding of Al 6082 alloy by AC pulse-GMA and AC wave pulse-GMA welding,” *Materials and Design,* pp. 306-313, April 2009.

[66] “Weld metal composition change during conduction mode laser welding of aluminum alloy 5182,” *Metallurgical and Materials Transactions B,* pp. 163-172, February 2001.

[67] Introduction to Aluminum Alloys and tempers, ASM Internationa, 2000.

[68] ASM Handbook, Properties and Selection: Nonferrous Alloys and Special-Purpose Materials, vol. Volume 2, ASM International, 1992.

[69] H. Liu, T. Sparks and F. Liou, “Residual Stress and Deformation Modelling for Metal Additive Manufacturing Processes,” in *Proceedings of the World Congress on Mechanical, Chemical, and Material Engineering*, Barcelona, Spain, 2015.

[70] J. Mehnen, J. Ding, H. Lockett and P. Kazanas, “Design for Wire and Arc Additive Layer Manufacture,” *Proceedings of the 20th CIRP Design Conference, Ecole Centrale de Nantes, Nantes, France,* pp. 721-727, April 2010.

[71] S. Williams and J. Ding, “Wire and Arc Additive Manufacture (WAAM) software requirements and development plans,” Report for WAAMMat partners, 2016.

[72] F. Michel, H. Lockett, J. Ding and S. Williams, “WAAMSoft: Path Generator Framework for WAAM,” *Preprint submitted to : Robotics and Computer-Integrated Manufacturing,* 28 February 2018.

[73] C. Lindemann, U. Jahnke and M. Moi, “Analysing product lifecycle costs for a better understanding of cost drivers in additive manufacturing,” *Twenty Third Annual Inernational Solid Freeform Fabrication Symposium,* 2012.

[74] G. Venturini, F. Montevecci, A. Scippa and G. Campatelli, “Optimization of WAAM deposition patterns for T-crossing features,” *Optimization of WAAM deposition patterns for T-crossing features,* pp. 95-100, 2016.

[75] H. Chen, “Process study of Al alloy WAAM with AC plasma,” Cranfield university, 2016/17.

[76] Metals Handbook Desk Edition, ASM International, 1998.

[77] CUI INC, “Design considerations for thermal management of power supplies,” 11 2014. [Online]. Available: https://www.cui.com/catalog/resource/design-considerations-for-thermal-management-of-power-supplies.pdf. [Accessed 07 April 2018].

[78] S. H. Oliari, A. S. C. M. D'Oliveira and M. Schulz, “Additive Manufacturing of H11 with Wire-Based Laser Metal Deposition,” *Soldagem & Inspeção,* vol. 22, pp. 466-479, 2017.

[79] V. R. Duarte, “Additive manufacturing of a high resistance steel by MIG/MAG,” Master of Science Thesis, Faculdade de Ciências e Tecnologia, Lisboa, 2016.

[80] W. Aiyiti, W. Zhao, B. Lu and Y. Tang, “Investigation of the overlapping parameters of MPAW-based rapid prototyping,” *Rapid Prototyping Journal,* vol. 12, pp. 165 - 172, 2006.

[81] G. Venturi, F. Montevecchi, A. Scippa and G. Campatelli, “Optimization of WAAM deposition patterns for T-crossing features,” *Procedia CIRP,* pp. 95-100, 2016.

[82] J. Fu, K. Qiu, L. Gong, C. Liu, Q. Wu, J. Lu and H. Fan, “Effect of Tool-Path on Morphology and Mechanical Properties of Ti-6Al-4V Fabricated by Wire and Arc Additive Manufacturing,” *MATEC Web of Conferences,* p. 128, 2017.

[83] J. Lin, Y. Lv, Y. Liu, Z. Sun, K. Wang and Y. Wu, “Microstructural evolution and mechanical property of Ti-6Al-4V wall deposited by continuous plasma arc additive manufacturing without post heat treatment,” *Journal of the Mechanical Behavior of Biomedical Materials,* pp. 19-29, 2017.

[84] T. Udomphol, “Weld microstructure-Suranaree University of Technology,” September 2007. [Online]. Available: http://eng.sut.ac.th/metal/images/stories/pdf/04_Weld%20microstructure01.pdf. [Accessed 2018 April 20].

[85] J. Gu, B. Cong, J. Ding, S. Williams and Y. Zhai, “Wire + Arc Additive Manufacturing of Aluminium,” in *Solid freeform fabrication symposium*, Austin, Texas, 2014.

[86] E. Gharibshahiyan, A. H. Raouf, N. Parvin and M. Rahimian, “The effect of microstructure on hardness and toughness of low carbon welded steel using inert gas welding,” *Materials and Design,* pp. 2042-2048, 2011.

[87] 3D Hubs, “What is 3D Printing?,” [Online]. Available: https://www.3dhubs.com/what-is-3d-printing. [Accessed 02 04 2018].

[88] ASM International, Corrosion: Understanding the basics, J. Davis, Ed., ASM International, 2000.

[89] E. Yasa, O. Poyraz, E. Solakoglu, G. Akbulut and S. Oren, “A study on the stair stepping effect in direct metal laser sintering of a nickel-based superalloy,” *3rd CIRP Conference on Surface Integrity ,* pp. 175-178, 2016.

[90] S. O. Onuh and Y. Y. Yusuf, “Rapid prototyping technology: applications and benefits for rapid product development,” *Journal of Intelligent Manufacturing ,* pp. 301-311, 1999.

7 Appendix

Appendix A – Grinding and polishing guide steps for aluminium.

For the analysed samples, the following procedure were followed:

1) Grinding
    i. Remove the samples out of the mould;
    ii. Grind the opposite surface with sandpaper 240 to flatten the bottom;
    iii. Grind the surface of interest with sandpaper 240;
        a. Until the surface of the sample is reaches;
    iv. Grind the sample with sandpaper 1200;
        a. Apply for two minutes;
        b. Repeat with another sandpaper;
    v. Grind the sample with sandpaper 2500;
        a. Apply for 2 minutes;
        b. Repeat with another sandpaper;
2) Polishing
    i. Use aluminium plate with magnetic surface of 6 microns;
        a. Apply 6 microns suspension for 3 minutes;
    ii. Use aluminium plate with magnetic surface of 3 microns;
        a. Apply 3 microns suspension for 3 minutes;
    iii. Use 0,5 microns plate with polishing alumina suspension;
        a. Apply for 3+3 minutes (clean disc in between);
        b. If the surface still has scratches, do iii again;
    iv. Wash the 0,5 microns plate and use the OPS suspension;
        a. Apply for 6 minutes.
3) Etching
    i. The etching was performed using Kellers etchant for 10 seconds.

Appendix B – Deposition code of section 1 to implement in the robot for part S3 production.

```
<Building_Strategies>
  <Building_Strategy Name="BS 1">
    <Section Name="Section 1" Type="Sec_Oscill">
      <StepOver Unit="mm">3.5</StepOver>
      <ReduceOscill Unit="mm">0</ReduceOscill>
      <StartOffset Unit="mm">0</StartOffset>
      <EndOffset Unit="mm">0</EndOffset>
      <SplitLenghtStarts Unit="mm">10</SplitLenghtStarts>
      <SplitLenghtEnds Unit="mm">10</SplitLenghtEnds>
      <CoolingTime Unit="s">45</CoolingTime>
      <RollingGap Unit="mm">3</RollingGap>
      <RollingOffset Unit="mm">0</RollingOffset>
      <PP_Layer Name="L1" Type="PPL_Oscill">
        <Move Name="Z1" Type="Job" Color="Yellow">
          <TravelSpeed Unit="mm/s">3</TravelSpeed>
          <Approximation Unit="mm">1</Approximation>
          <JobNumber Unit="">1</JobNumber>
        </Move>
        <Move Name="Z2" Type="Job" Color="Blue">
          <TravelSpeed Unit="mm/s">3</TravelSpeed>
          <Approximation Unit="mm">1</Approximation>
          <JobNumber Unit="">1</JobNumber>
        </Move>
        <Move Name="Z3" Type="Job" Color="Red">
          <TravelSpeed Unit="mm/s">3</TravelSpeed>
          <Approximation Unit="mm">1</Approximation>
          <JobNumber Unit="">1</JobNumber>
        </Move>
      </PP_Layer>
```